Geomechanics and Engineering, *Vol. 31*, *No. 1 (2022) 31-52*
https://doi.org/10.12989/gae.2022.31.1.031

Evaluating effects of various water levels on long-term creep and earthquake performance of masonry arch bridges using finite difference method

Murat Cavuslu*

Department of Civil Engineering, Zonguldak Bulent Ecevit University, Zonguldak, Türkiye

(*Received January 13, 2022, Revised August 29, 2022, Accepted September 14, 2022*)

Abstract. Investigating and evaluating the long-term creep behavior of historical buildings built on seismic zones is of great importance in terms of transferring these structures to future generations. Furthermore, assessing the earthquake behavior of historical structures such as masonry stone bridges is very important for the future and seismic safety of these structures. For this reason, in this study, earthquake analyses of a masonry stone bridge are carried out considering strong ground motions and various water levels. Tokatli masonry stone arch bridge that was built in the 10th century in Turkey-Karabük is selected for three-dimensional (3D) finite difference analyses and this bridge is modeled using FLAC3D software based on the three-dimensional finite difference method. Firstly, each stone element of the bridge is modeled separately and special stiffness parameters are defined between each stone element. Thanks to these parameters, the interaction conditions between each stone element are provided. Then, the Burger-Creep and Drucker-Prager material models are defined to arch material, rockfill material for evaluating the creep and seismic failure behaviors of the bridge. Besides, the boundaries of the 3D model of the bridge are modeled by considering the free-field and quiet boundary conditions, which were not considered in the past for the seismic behavior of masonry bridges. The bridge is analyzed for 6 different water levels and these water levels are 0 m, 30 m, 60 m, 70 m, 80 m, and 90 m, respectively. A total of 10 different seismic analyzes are performed and according to the seismic analysis results, it is concluded that historical stone bridges exhibit different seismic behaviors under different water levels. Moreover, it is openly seen that the water level is of great importance in terms of earthquake safety of historical stone bridges built in earthquake zones. For this reason, it is strongly recommended to consider the water levels while strengthening and analyzing the historical stone bridges.

Keywords: burger-creep material model; earthquake analysis; free-field boundary condition; masonry arch bridge; water level

1. Introduction

Water is of great importance for people to continue their lives. For this reason, it is necessary to protect water resources to preserve the health and safety of humanity. However, flood disasters have many negative effects on historical structures. Especially the exposure of historical structures such as bridges to flood disasters can cause serious damage to these structures. For this reason, it is necessary to strengthen the centuries-old historical bridges against floods and to make these structures ready for flood disasters. In the literature, long-term creep and three-dimensional seismic behaviors of historical stone arch bridges have never been investigated considering different water levels. One of the researchers who pioneered studies on the seismic behavior of historical bridges is Spyrakos *et al*. (1999). They created a three-dimensional model of a historical bridge and the material parameters of the bridge were acquired from in-situ ultrasonic tests. According to static deflection results, the maximum deflection value under dead loads is 10.87 mm. Moreover, the maximum deflection value under live loads is 18.36 mm. Jiang and Esaki (2002) examined the structural behavior of the historical arch bridges under physical and chemical weathering conditions. A distinct element method was utilized while modeling the bridge and a 16-ton dead load was subjected to the bridge. Arch elements were presumed as elastic. According to numerical analyses, the maximum displacements occurred in the middle of the arch section. Ural *et al*. (2008) assessed the failure behavior of the masonry arch bridges in Turkey. The important damage situations in the masonry bridges such as earthquake damage and hydrostatic damage were evaluated and it was concluded that flood damage strongly affects the structural behavior of the bridges. Pelà *et al*. (2009) examined the earthquake performance of the masonry bridges using UNI ENV 1998-1 2003, FEMA 440 2005, and OPCM 32742004 standards. Experimental and numerical analyses were performed for the Marcello Pistoiese bridge and Cutigliano bridge. Mechanical properties of the bridge were acquired using compression tests. According to three-dimensional numerical analyses, the frequency of the mode for the Marcello Pistoiese Bridge is 3.998 Hz. Besides, the frequency of the mode for the Cutigliano Bridge is 23.1 Hz. Milani and Lourenço (2012) investigated the structural behavior of the masonry arch bridges. Firstly, three-dimensional modeling was performed and interface

*Corresponding author, Ph.D.
E-mail: murat.cavusli@beun.edu.tr

ISSN: 2005-307X (Print), 2092-6219 (Online)

elements were defined to the discrete surfaces using the k_{t1} and k_{t2} parameters. According to numerical analyses, critical deformations were observed in the arch section of the bridge using the distinct element and the applied element methods. Domede *et al*. (2013) assessed the structural failure performance of a 20th-century masonry bridge considering numerical modeling and experimental tests. Mechanical parameters of the bridge were obtained by taking into account compression tests. Then, a three-dimensional model of the bridge was created utilizing railway loads and 3.5 mm maximum displacements were gained on the arch section of the bridge. Pelà *et al*. (2013) compared relationships between the earthquake evaluation procedures for historical arch bridges. A total of 84 earthquake analyses were performed and critical pseudo accelerations occurred on the arch bridge. Furthermore, 0.021 m maximum displacement was observed in the masonry arch bridge. Gonen *et al*. (2013) evaluated the structural failure performance of historical arch bridges. Three-dimensional analyses of the Murat arch bridge were performed under dead loads and linear elastic earthquake loads. According to numerical analyses, it was concluded that failure mechanisms of the masonry arch bridges progress more rapidly than in other historical buildings. Dogan (2013) investigated the structural failure behavior of the RC masonry bridges using the 23 October 2011 Van Earthquake. It was concluded that many critical failures occurred in the masonry bridges during the Van earthquake. Costa *et al*. (2015) performed a study on the modeling four various masonry arch bridges using the finite element method and discrete element method. Deformability and strength parameters of the bridge materials were obtained from the experimental tests and numerical analyses were examined under static loads. Good correlations were obtained between the three-dimensional analyses and the hinge mechanism. Hacıefendioğlu and Koç (2016) evaluated the earthquake performance of the historical arch bridges under blast-induced ground motion using the multi-point shock spectrum method. It was assessed the damaged and restored situations of the bridge. A three-dimensional model of the bridge was created and it was seen that the frequency (first mode) of the restored bridge is 3.02 Hz. Conde *et al*. (2016) examined the structural behavior of the historical arch bridges taking into account the arch geometry and rockfill material. According to three-dimensional analyses of the Monforte de Lemos bridge, critical damages occurred in the arch section of the bridge with nonlinear and real geometry. Karaton *et al*. (2017) performed earthquake failure analyses of a masonry bridge under various strong ground motions. Material parameters were obtained using compression tests and a three-dimensional model was created considering the original bridge project. According to numerical analyses, it was concluded that the frequency (first mode) of the bridge is 3.6935 Hz. Tubaldi *et al*. (2018) investigated the mesoscale analyses of the historical arch bridges. According to numerical analyses, good correlations were acquired between numerical and experimental results. Moreover, it was proposed that mesoscale modeling can be utilized to perform three-dimensional numerical analyses of various bridges. Aydin and Özkaya (2018) examined the three-dimensional behavior of the Sarpdere masonry arch bridge using the ANSYS software. According to the numerical analysis results, it was seen that the total maximum load-carrying capacity of the bridge is 48.97 t/m. Sarhosis *et al*. (2019) modeled a historical arch bridge using a discrete element method. It was assumed that k_n and k_s parameters that are mortar joint interface parameters between distinct surfaces are 35 GPa/m and 7 GPa/m, respectively. According to numerical analyses, important failure damages were observed in the arch section of the bridge. Cakir and Seker (2015) examined the structural failure performance of a masonry bridge and static, modal, and nonlinear earthquake analyses were performed. According to numerical analyses, critical failure damages were observed in the arch material of the bridge. Türker (2014) evaluated the structural failure behavior of the Aspendos historical arch bridge. A new model was proposed to the literature for the masonry bridges and this model was calibrated according to ambient vibration test results. Yazdani *et al*. (2019) assessed the seismic performance of concrete arch bridges under near-field earthquakes using incremental dynamic analysis. It was seen that the near-field seismic performance of the masonry arch bridge with a lower span length (5L06 bridge) is safer than the bridge with a longer span length (2L20 bridge). Yazdani and Jahangiri (2020) performed intensity measure-based probabilistic seismic evaluation and vulnerability assessment of ageing bridges. The numerical results showed that decreasing the span length of the arch bridges causes the increase in the return period of exceeding various limit states. Panian and Yazdani (2020) performed an estimation of the service load capacity of plain concrete arch bridges taking into account the stress intensity factor. For validating the results, two arch bridges were used and the results revealed that the proposed method agreed well with the field observations. Yazdani and Habibi (2021) performed the residual capacity evaluation of masonry arch bridges using the extended finite element method (XFEM). The numerical results showed that XFEM agrees very well with the other methods. Moreover, it was indicated that XFEM can be employed effectively and efficiently to analyze ageing cracked masonry arch bridges. Yazdani (2021) performed the three-dimensional numerical analyses of a railway arch bridge to predict load-carrying capacity using the three-dimensional finite element method. The numerical results indicated that the load-carrying capacity of the 2PL20 bridge equals 8880 kN under the static field test. Besides, there are many studies about assessing seismic failure mechanisms of the masonry arch bridges in the literature such as Sayin (2016), Zampieri *et al*. (2021), Saygılı and Lemos (2021), Forgács *et al*. (2021), Gönen and Soyöz (2021), Onat (2019). It is seen from these studies that the effects of various water levels on the nonlinear seismic behavior of the masonry arch stone bridges were not examined in the past. Furthermore, the Burger-creep material model and non-reflecting boundary conditions were not used for assessing of long-term creep and seismic behaviors of the historic stone bridges. For this reason, this study provides to close the deficiencies in the literature.

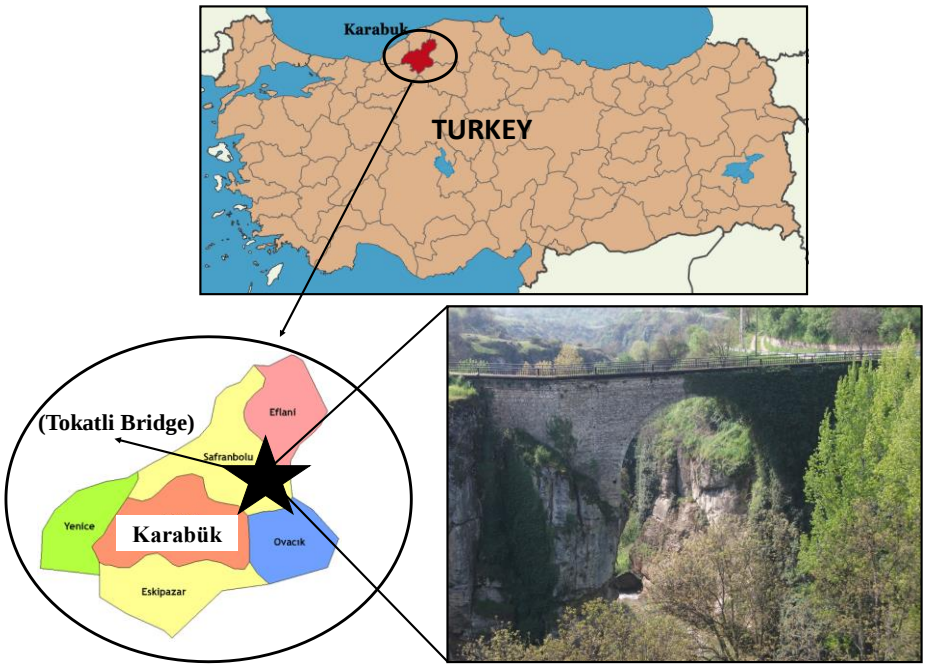

Fig. 1 Location of the Tokatli bridge (Yeşil 2019)

2. Scope and originality of the study

Floods can cause material failures in historical buildings. For this reason, it is vital to examine the effects of these critical damages on the creep and seismic behavior of important structures that are in constant contact with water such as historical bridges. In this study, the effects of different water levels on the creep and seismic behavior of the historical Tokatli bridge are evaluated in detail. Firstly, the three-dimensional finite difference model of the bridge is created by considering the discrete modeling. Each stone element of the bridge is modeled separately and special stiffness parameters are defined between each stone element. Thanks to these stiffness parameters, the interaction conditions between the discrete elements of the historical bridge have been acquired. The first aim of this study is to examine the long-term creep and seismic behaviors of the historical bridges modeled using the discrete element method and to determine the effects of stiffness parameters defined between discrete elements on the earthquake behavior of historical bridges. Furthermore, the creep and seismic behavior of the bridge is assessed by taking into account the Burger-Creep material model, which was not used for the creep behavior of historical bridges in the past. The second aim of this study is to determine the effects of the Burger-Creep material model on the creep and seismic behavior of historical stone arch bridges under 10 various ground motions. The most important aim of this study is to determine the effects of critical disasters such as floods and overflows on the long-term creep and seismic failure behavior of historical bridges. For this purpose, a total of 6 different water levels (0 m, 30 m, 60 m, 70 m, 80 m, and 90 m) are taken into account in creep and seismic analyses. As a result of this study, the effects of different water levels on the seismic behavior of historical stone bridges have been revealed, and thanks to this study, important information about the effects of the flood on the structural behavior of the masonry stone bridges is ensured in the literature. Finally, a total of 10 various strong ground motions are used in the nonlinear seismic analyses.

3. General information about Tokatli Bridge and 3D nonlinear modelling

Tokatli historical bridge was built in 1179. Its body and arch were created from stone elements. This bridge, which has been exposed to water loads for years, has managed to survive until today. This important masonry structure' length and width are 40 m and 6 m, respectively. The span of the bridge is 15 m and its' height is 30 m. The general view of the bridge is shown in Fig. 1. The bridge was located in the northern part of Turkey. Besides, the two-dimensional view of the bridge is shown in Fig. 2.

The finite difference method is by far the easiest numerical method to understand and implement when tackling differential equations, for problems that satisfy its structured discretization assumptions. Thanks to this method, discrete modeling of important structures such as bridges, interaction modeling, boundary condition modeling, static and dynamic analyses can be done easily. Moreover, the finite difference method used by the FLAC3D program provides researchers with specific material models and boundary conditions for geotechnical problems. For this reason, in this study, the finite difference method is used for the numerical analyses of historical stone bridges, unlike the literature. Firstly, the arch section of the bridge is created and each stone element in the arch section is modeled separately (Fig. 3). Interaction stiffness coefficients are defined between the interaction surfaces of the stone elements by considering the k_n and k_s coefficients (Cavuslu 2022). After the three-dimensional model of the

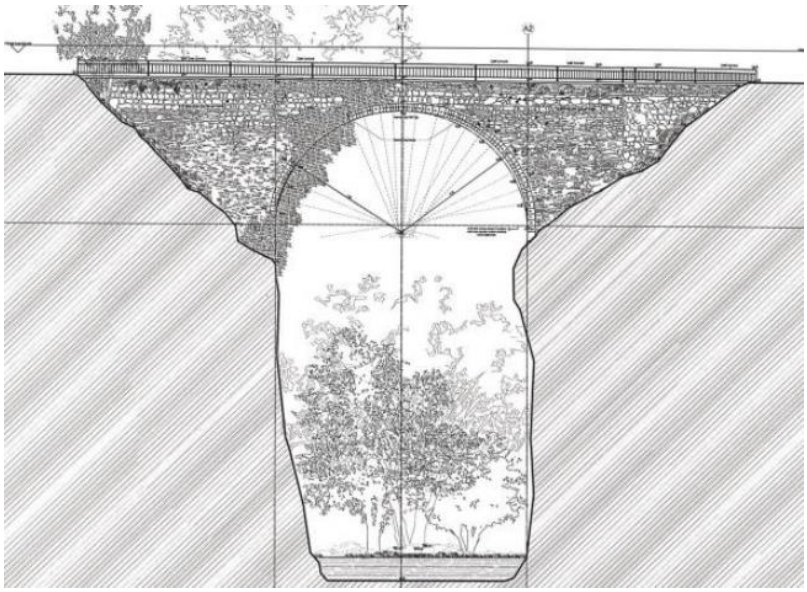

Fig. 2 Original project of the Tokatli bridge (Yeşil 2019, Cavuslu 2022)

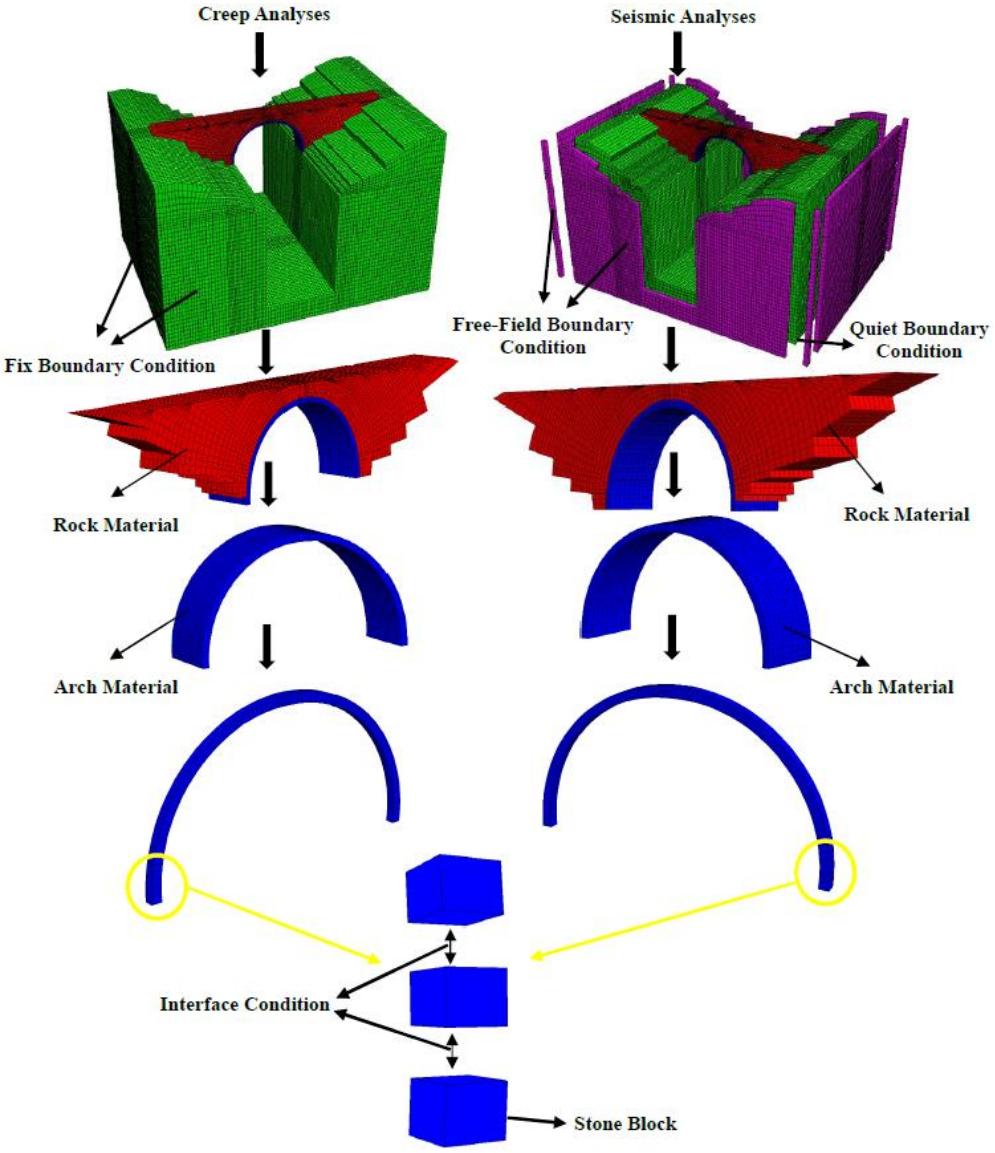

Fig. 3 3D model of the Tokatli bridge

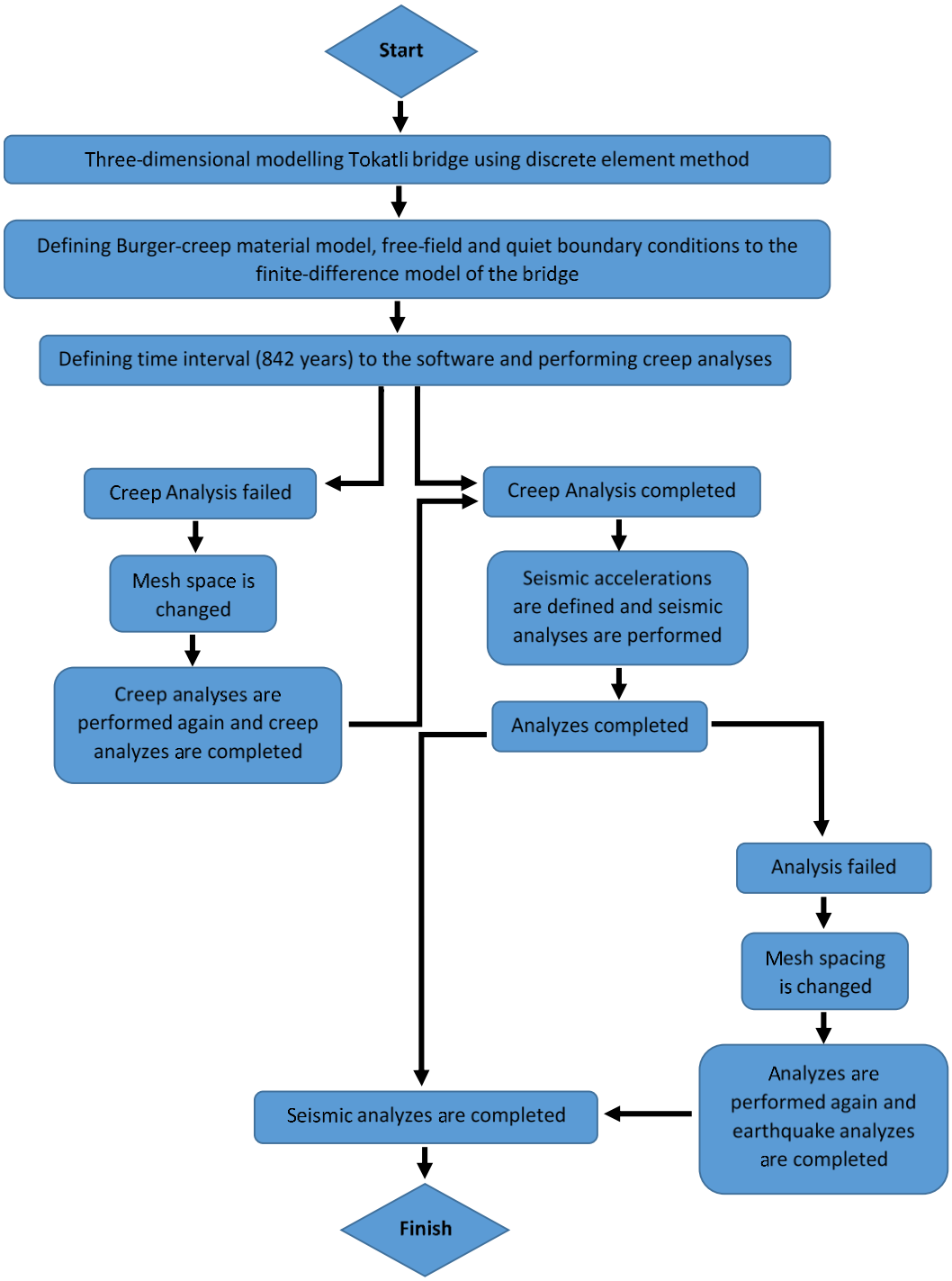

Fig. 4 Analysis chart for numerical analyses of the Tokatli bridge

Table 1 Summary of the nonlinear material properties of the Tokatli bridge (Yeşil 2019)

Material Property	Arch Material	Rockfill Material	Foundation
E	6.9 (GPa)	6.1 (GPa)	1.32 (GPa)
f_c	6.8 (MPa)	5.9 (MPa)	1.4 (MPa)
f_t	0.91 (MPa)	0.84 (MPa)	0.17 (MPa)
V_{st}/V_{mo}	0.98/0.09	0.93/0.14	N/A
γ	27.15 (kN/m^3)	26.42 (kN/m^3)	20.03 (kN/m^3)
μ	0.25	0.24	0.29

bridge is created, the fix (reflecting) boundary condition is defined in the z-direction at the base of the bridge for creep analyses. For the seismic analyses, quiet (non-reflecting) boundary condition is defined at the base of the model (Fig. 3). The behavior of non-linear materials is considered in modeling the Tokatli bridge. In this order, the Burgers-Creep criterion is utilized for the arch and rockfill. Moreover, the Drucker-Prager criterion was used for the foundation (Yazdani and Jahangir 2020). To apply the Burgers-Creep criterion, it is essential to calculate the acquired values for input data, including modulus of

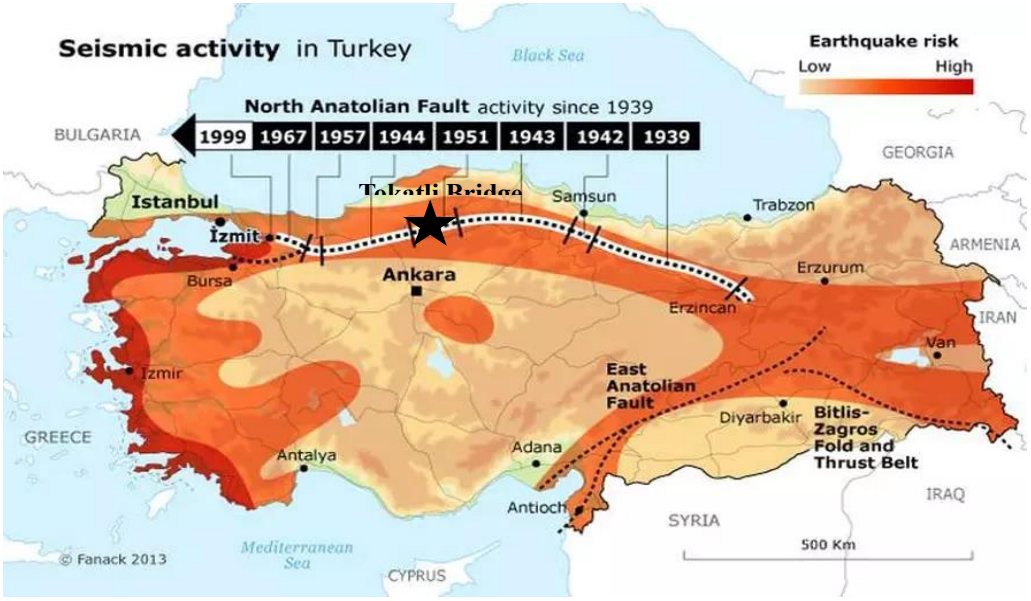

Fig. 5 The fault map of Turkey (Fanack 2022)

Table 2 Mechanical characteristics of ground motions (PEER 2022)

Case	Earthquake	M_w	Distance (km)	A_p (g)	V_p (cm/s)	T_p (s)
1	1983 Borah Peak	6.9	36	0.79	108	7.8
2	1992 Cape Mendocino	6.6	44	1.53	152	9.4
3	1999 Chi-Chi (2)	7.6	22	0.62	107	8.5
4	1981 Gulf of Corinth	6.5	27	0.59	94	7.3
5	1979 Imperial Valley	6.5	42	0.41	85	8.2
6	1995 Kobe	6.9	53	0.48	94	7.1
7	1999 Kocaeli	7.2	49	0.49	90	7.6
8	1995 Kozani	6.6	71	0.45	86	7.0
9	2012 Emilia-Italy	6.0	57	0.55	101	7.4
10	1967 Borrego Mountain	6.6	34	0.50	91	7.2

Table 3 Various situations of Tokatli bridge for creep and seismic analyses

Situation	Water Level (m)
1	0
2	30
3	60
4	70
5	80
6	90

elasticity (E), compressive strength (f_c), tensile strength (f_t), volumetric ratio (V_{st}/V_{mo}), specific weight (γ) and poisson's ratio (μ) (Table 1). This criterion was created by combining a Kelvin model and Maxwell model. Then, elasticity modulus (E), Poisson ratio (υ), cohesion (c), friction coefficient (ϕ), and dilation angle (ψ) is used to apply the Drucker-Prager criterion. The Burgers-creep model is a rheological model that is consistent with the rheological properties of the slip surface. It can reflect the transient and attenuation stages of creep deformation (Wang *et al.* 2020).

This model in FLAC is characterized by a visco-elastoplastic deviatoric behavior and an elastoplastic volumetric behavior. The visco-elastic and plastic strain-rate components are assumed to act in series (Cavuslu 2022). The visco-elastic constitutive law corresponds to a Burger model (Kelvin cell in series with a Maxwell component), and the plastic constitutive law corresponds to a Mohr-Coulomb model. This model is capable of accurately describing the creep law of rocks above long-term strength (Karalar and Cavuslu 2022). This material model, which has never been used for creep analysis of masonry bridges in the literature, is used in this study to examine the creep and seismic behavior of the Tokatli masonry stone arch bridge. In the seismic analyses, a total of 10 different earthquakes are used and the mechanical properties of these earthquakes are shown in Table 2 in detail.

After the three-dimensional finite difference model of the bridge is created, the creep analysis of the bridge is performed (Fig. 4). A time interval (843 years) is defined to the FLAC3D software and the creep behavior of the bridge is examined along 843 years. During the creep analyses, the software gave errors many times, and the reason for these errors is that the program does not accept the mesh range of the three-dimensional model. For this reason, the mesh range of the three-dimensional model of the bridge is changed many times. After the creep analyses, the seismic behavior of the bridge is examined for 2022. The Tokatli bridge is located on the northern anatolian fault line of Turkey (Fig. 5). Therefore, it is vital to examine the seismic behavior of this historic bridge.

In the seismic analyses, the software gave errors many times again, and therefore, the three-dimensional mesh space of the bridge is changed again for seismic analyses.

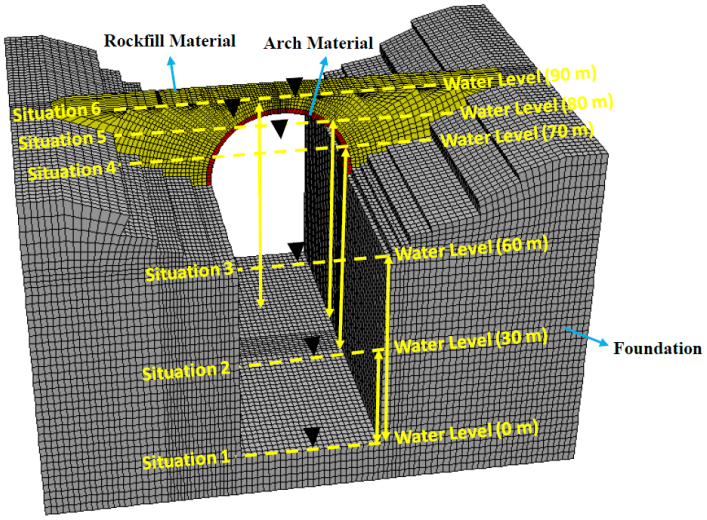

Fig. 6 Views of various water levels on the Tokatli historical stone bridge

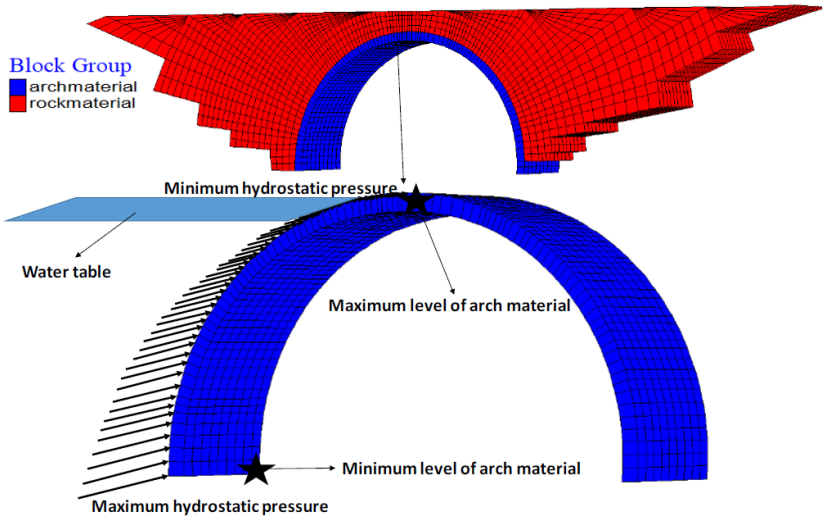

Fig. 7 View of how the reservoir water is affected on the bridge

For the creep and seismic analyzes of the bridge, 6 different water heights are taken into account and these water heights are shown in Table 3 in detail. While reservoir water is defined to the water holding surfaces of the bridge, firstly, hydrostatic water loads are defined on these surfaces of the bridge. The water loads are calculated depending on the height of the bridge and the water loads are increased proportionally from the upper elevations of the bridge to the lower elevations. Then, water tables are defined on the bridge depending on the water height. In Fig. 6, the general view of the water heights defined in the three-dimensional model of the bridge is shown in detail. According to Fig. 6, situation 1 represents the bridge's empty reservoir situation. Also, situation 6 represents the full reservoir situation of the bridge. Moreover, a view of how the reservoir water is affected on the bridge is shown in Fig. 7.

4. Three dimensional creep and seismic analysis results

In this section, the long-term creep and three-dimensional (3D) seismic analyses of the Tokatli masonry stone arch bridge are assessed in detail. In general, according to the creep and seismic analysis results, it is observed that various water levels significantly changed the structural behavior of stone bridges. In Fig. 8, 843 years' creep behavior of the Tokatli bridges is evaluated in detail. For the full reservoir condition of the bridge, the maximum vertical displacements occurred in the middle parts of the arch material (Fig. 8(a)). Approximately 6 cm maximum displacement is observed in the middle sections of the bridge over 843 years. Furthermore, it is concluded that significant creep cracks took place in the middle sections of the bridge, and the hydrostatic pressure excessively affected the structural behavior of the bridge's middle section for situation 6. In Fig. 8(b), the creep behavior of the bridge is examined for situation 5. According to Fig. 8(b), the greatest vertical displacements that occurred in the middle sections of the bridge during 843 years is about 5.2 cm. As the creep analysis is assessed for 843 years, it is openly seen

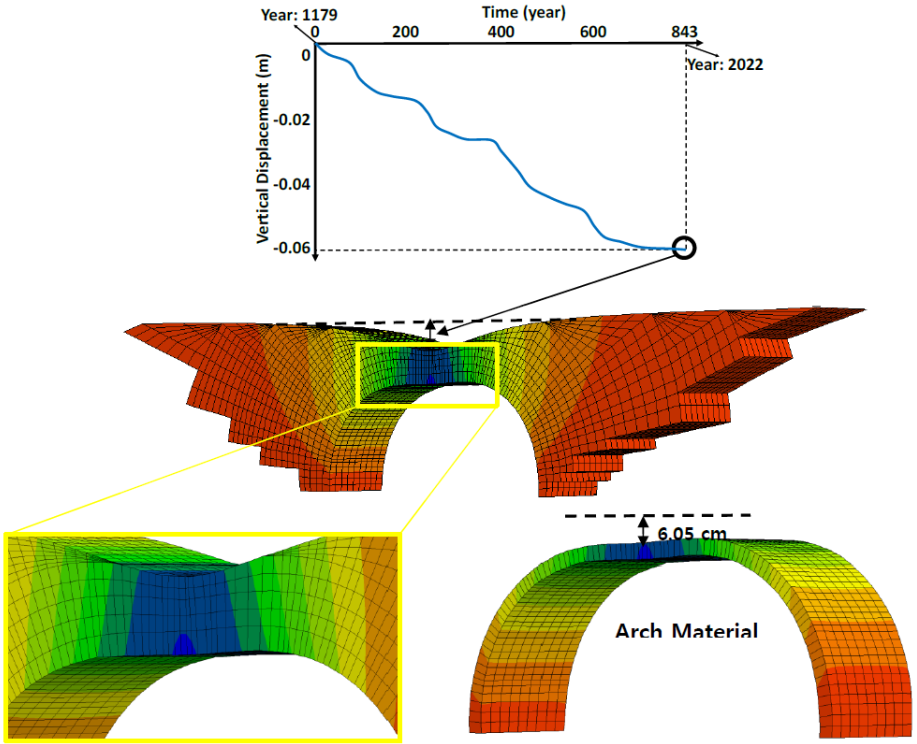

(a) Situation 6

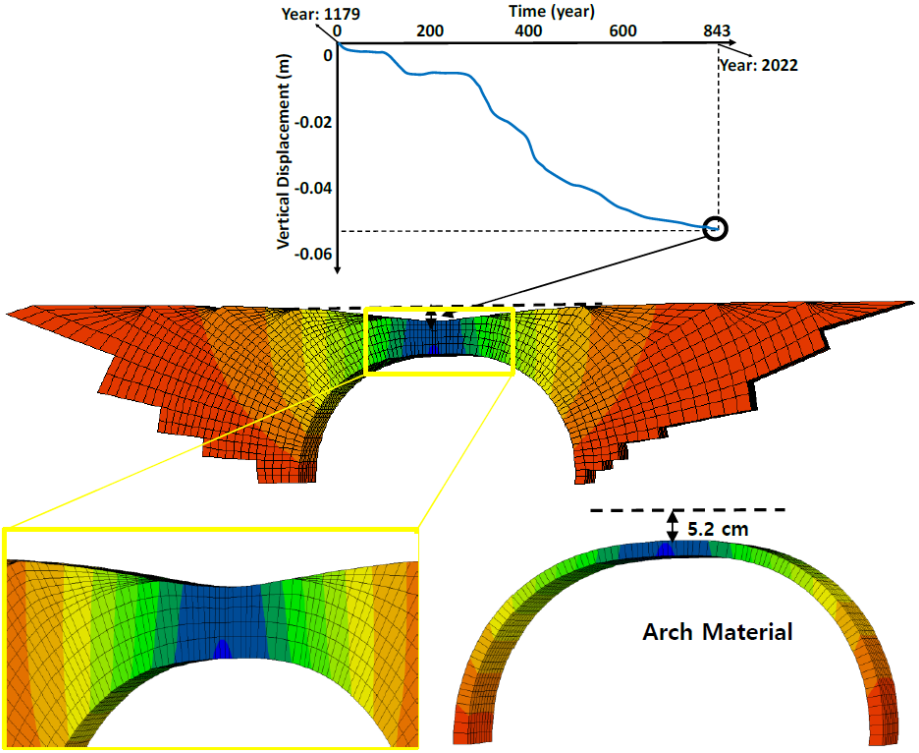

(b) Situation 5

Fig. 8 Long-term creep behavior of the bridge for different situations

that the increase rate of vertical displacements increased continuously for a certain period, but after a certain period, the increase rate of vertical displacements on the bridge decreased. In Fig. 8c, the creep analysis results obtained for situation 4 are presented in detail. According to Fig. 8(c), it is seen that the maximum vertical displacement value that took place in the middle sections of the bridge is approximately 4.05 cm. When Figs. 8(c) and 8(a) are compared with each other, the effects of hydrostatic pressure on the creep behavior of masonry bridges are clearly seen. In Fig. 8(d), the creep behavior of the bridge is examined for situation 3. According to Fig. 8(d), due to the

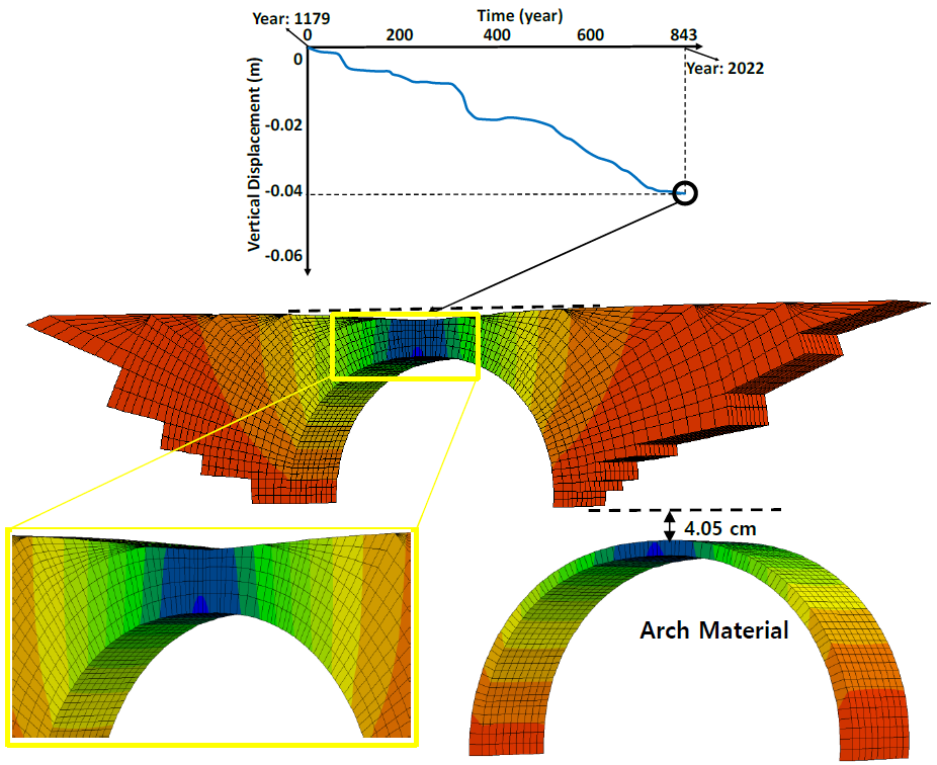

(c) Situation 4

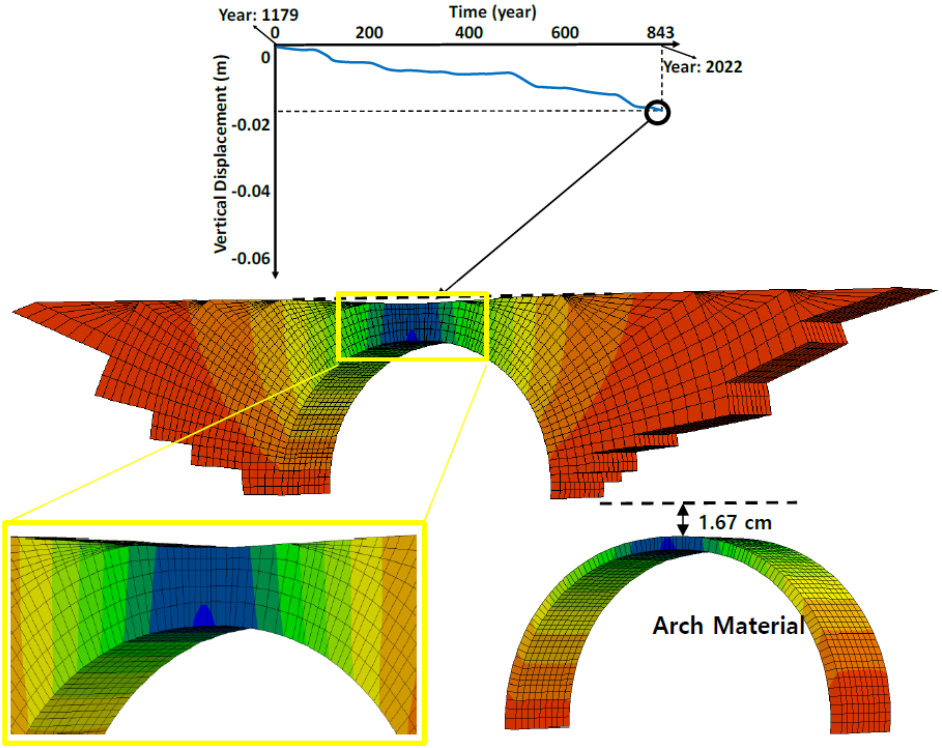

(d) Situation 3

Fig. 8 Continued

water loads not contacting the body surfaces of the bridge, very large vertical displacements have not occurred in the body of the bridge. Approximately 1.67 cm maximum vertical displacements have been observed in the middle sections of the bridge's arc material. Besides, it is seen that after 600 years, very few vertical displacement changes are observed in the middle parts of the bridge. In Fig. 8(e), the creep behavior of the bridge is presented for situation 2. According to Fig. 8(e), about 0.73 cm maximum vertical displacements are gained in the middle sections of the bridge for 843 years. No critical vertical displacements and cracks are observed in the bridge's body because the water

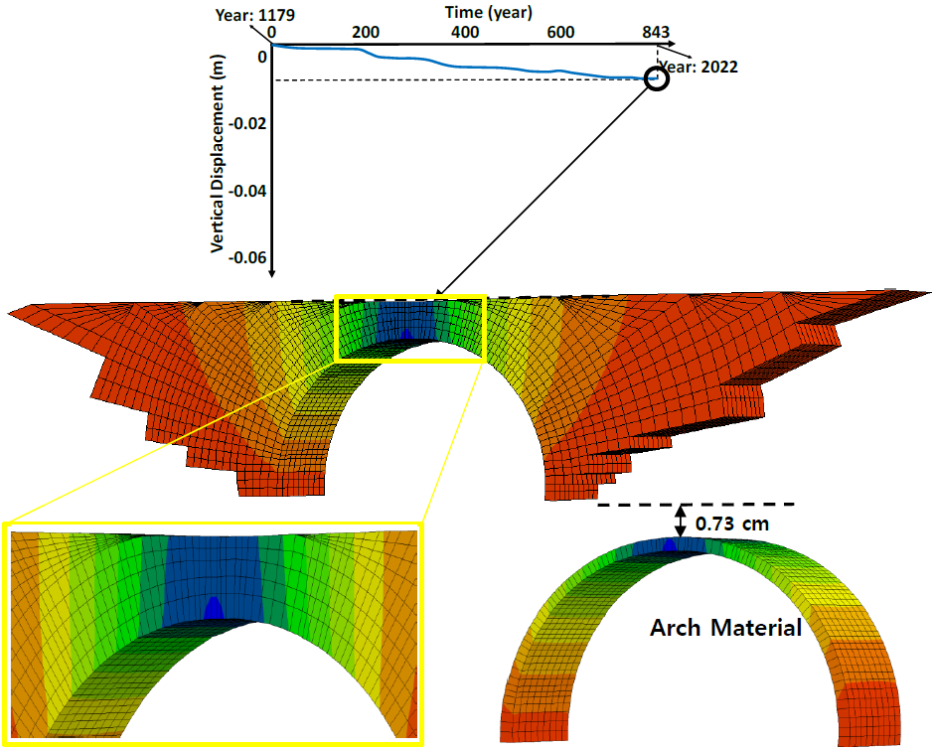

(e) Situation 2

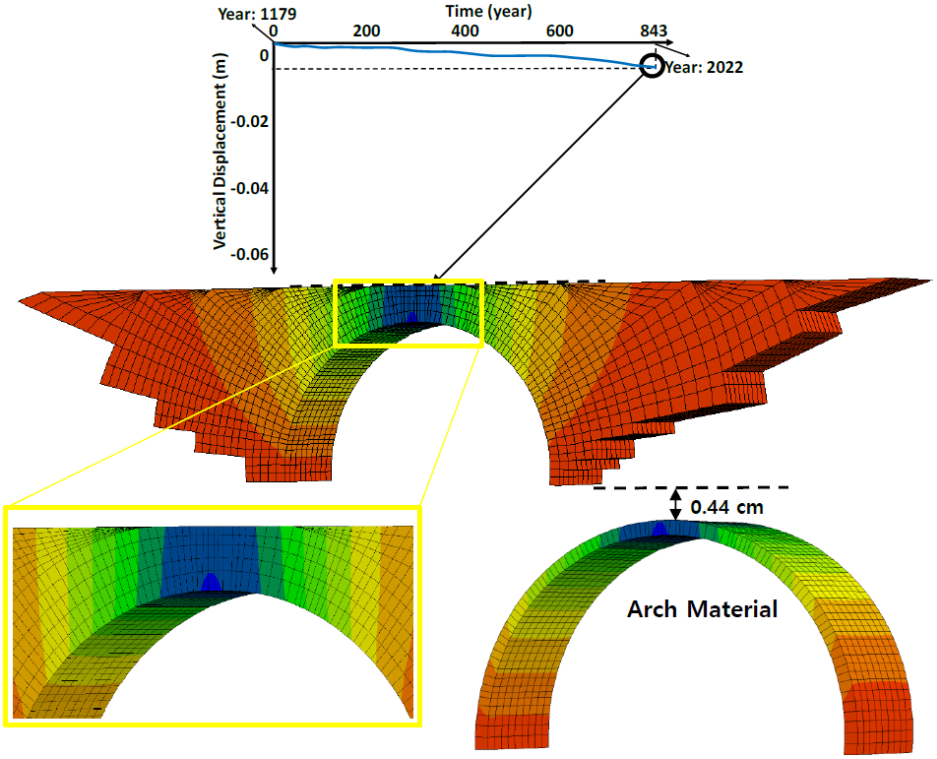

(f) Situation 1

Fig. 8 Continued

loads do not come into contact with the body of the bridge. In Fig. 8(f), the creep behavior of the bridge is presented for situation 1 and it is seen that the total vertical displacement on the bridge body during 843 years is 0.44 cm.

In Figs. 9-18, the seismic analysis results of the Tokatli stone arch bridge are presented in detail. Seismic analyzes are performed using 10 different ground motions and the time-depending vertical displacement results that occurred on the bridge's body are presented for 6 different water heights. Seismic analysis results for Case 1 are presented in Fig. 9. According to Fig. 9, the largest displacements on the bridge's body are observed for situation 6. Besides, the

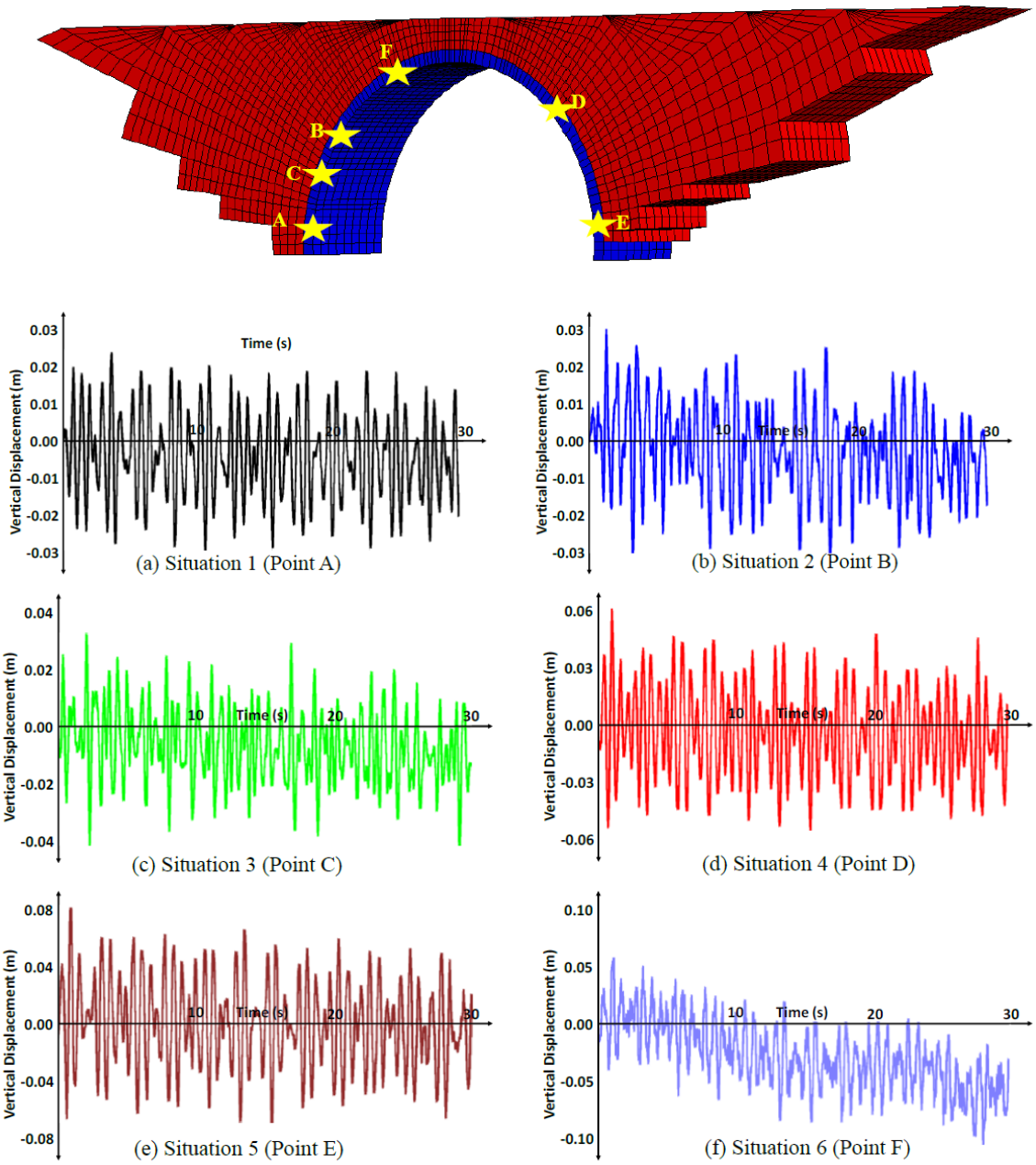

Fig. 9 Nonlinear seismic displacement results of the bridge for Case 1

smallest displacements on the bridge's body occurred in situation 1. From this result, the effects of changing water height on the seismic behavior of masonry stone arch bridges are clearly understood. For situation 1, the largest displacement value on the Tokatli bridge is 2.87 cm. Besides, 2.92 cm and 3.91 cm maximum vertical displacement values took place for situation 2 and situation 3, respectively. Similar seismic vertical displacement values on the bridge are obtained for situation 5 and situation 6. The most critical cracks for situation 6 are observed in the middle sections of the arch material (Fig. 9). This numerical result clearly shows that the most critical section of the bridge during the earthquake is the arch material. In Fig. 10, the seismic analysis results are shown for Case 2. According to Fig. 10, the largest vertical displacement on the bridge's body for situation 1 is 1.89 cm. Moreover, the maximum displacement values observed in the bridge body for situation 2, situation 3, and situation 4 are 2.92 cm, 4.88 cm, and 5.92 cm, respectively. It is seen that the largest displacement values on the bridge for situation 5 and situation 5 are larger than in other situations. The most critical cracks in the bridge for Case 2 are obtained around the arch material of the bridge. From these results, it is concluded that different water levels significantly change the seismic behavior of masonry stone arch bridges. In Fig. 11, the seismic displacement results are presented for Case 3. According to Fig. 11, it is seen that the maximum vertical displacement value that took place on the bridge for situation 1 is 2.72 cm. The maximum vertical displacement values on the bridge body for situation 2 and situation 3 are 2.93 cm and 5.94 cm, respectively. Furthermore, the largest displacement values observed on the bridge body for

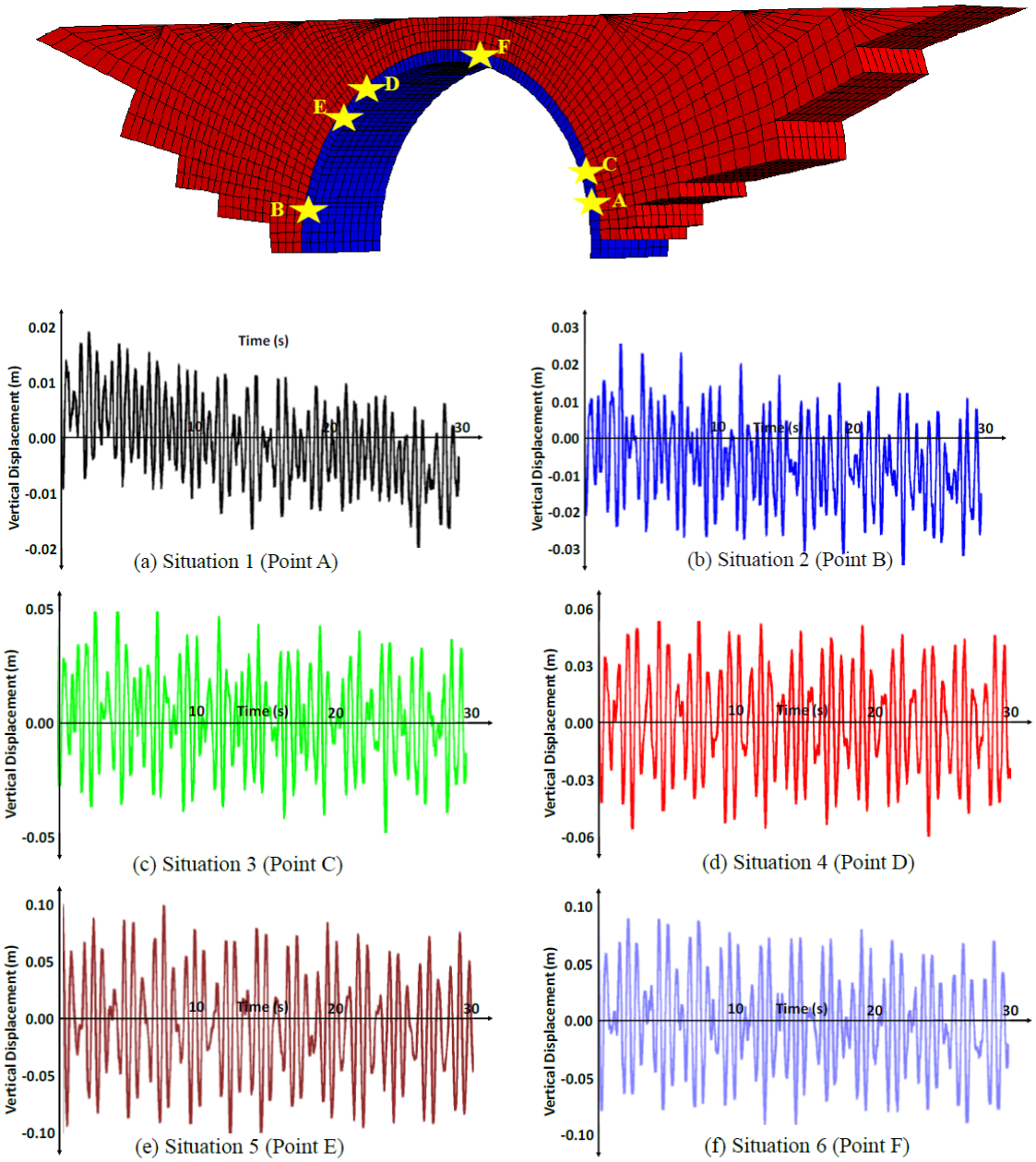

Fig. 10 Nonlinear seismic displacement results of the bridge for Case 2

situation 4, situation 5, and situation 6 are 7.89 cm, 9.91 cm, and 9.96 cm, respectively. From these results, it is inferred that as the water loads in contact with the bridge increase, the maximum displacement values that may occur during the earthquake increase significantly. The most critical displacement value for seismic safety of masonry stone bridges is 10 cm (Yazdani and Jahangiri 2020). If the maximum displacement value of the masonry bridges during the earthquake exceeds 10 cm, significant damage may occur to the bridge. In this study, for situations 1-3, seismic displacement values of less than 10 cm are obtained on the Tokatli masonry bridge during the earthquake. For this reason, no seismic damage occurred on the Tokatli bridge for 3 different water heights during the earthquake. However, since the maximum displacement values that occurred during the earthquake for situations 5 and 6 are close to 10 cm, it is suggested that earthquake reinforcement of the bridge should be performed for situation 5 and situation 6.

Fig. 12 shows the seismic analysis results of the bridge for Case 4. According to Fig. 12, it has been observed that the most critical section of the bridge is the middle part of the arch material section. During the earthquake, larger vertical displacements are acquired for situation 5 and situation 6 as compared to other situations. Besides, very close vertical displacement values are observed for situation 1 and situation 2. Maximum cracks are obtained in the middle section of the bridge for the full reservoir situation of the bridge (Fig. 12). For situation 1 and situation 2, the maximum vertical displacement values occurring on the Tokatli bridge are 1.82 cm and 2.92 cm, respectively. Besides, the maximum displacement values observed on the

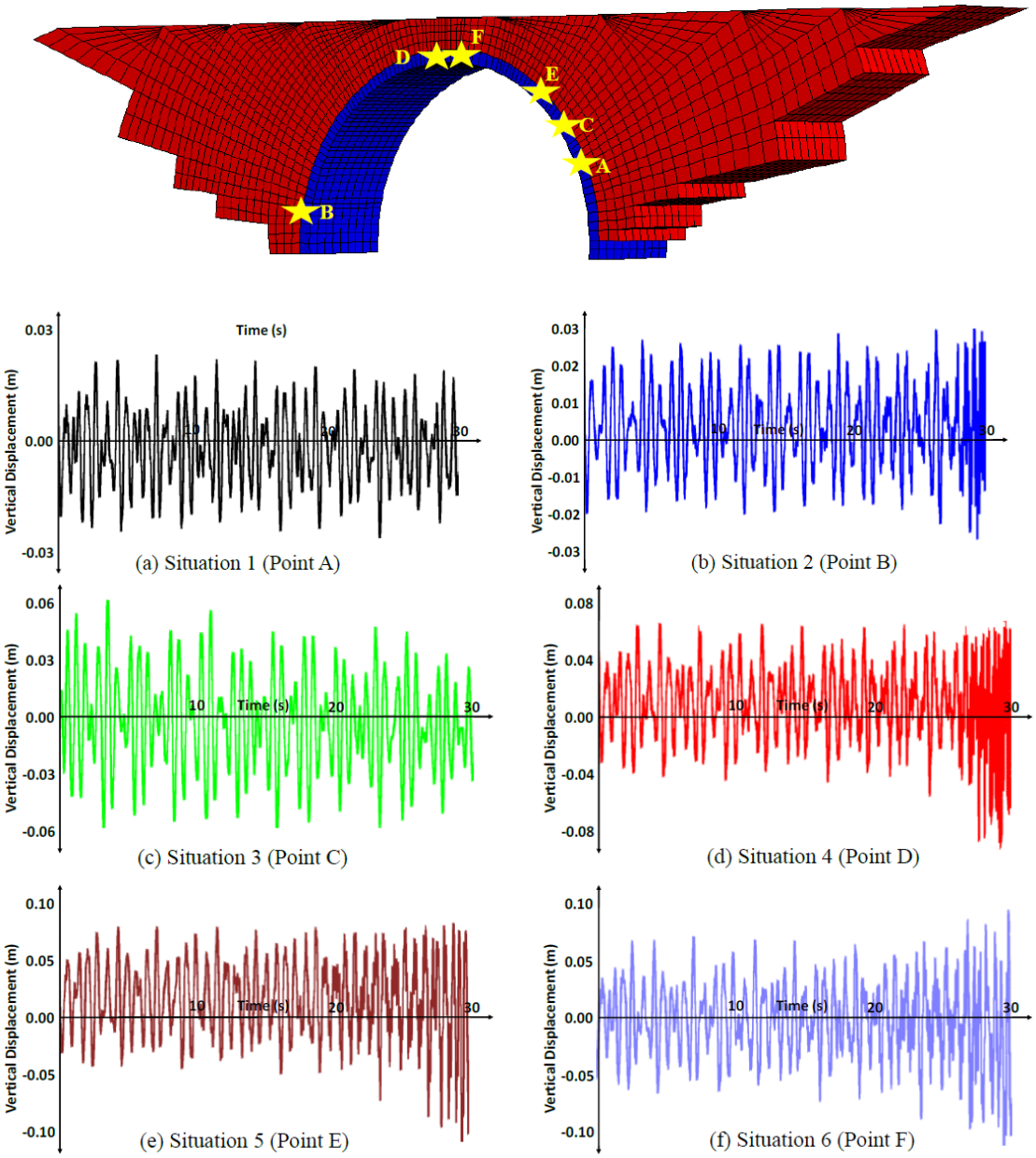

Fig. 11 Nonlinear seismic displacement results of the bridge for Case 3

bridge body for situation 3 and situation 4 are 5.89 cm and 7.96 cm, respectively. For Situation 6, the maximum vertical displacement on the bridge is greater than 10 cm, and it is concluded that this seismic displacement value can cause significant seismic damage to the bridge. In Fig. 13, the earthquake analysis results of the bridge are presented for Case 5. According to Fig. 13, 10.94 cm maximum vertical displacement is observed in the middle sections of the bridge body for the full reservoir condition. It is deduced that this seismic displacement value may cause significant seismic damage to the bridge. Moreover, it is seen that the vertical displacement values obtained for situation 6 are higher than the other situations and fewer vertical displacements are acquired on the bridge for situation 1 and situation 2 as compared with other situations. The maximum vertical displacement values on the bridge for situation 1 and situation 2 are 2.34 cm and 3.72 cm, respectively. Moreover, the largest seismic displacement values observed on the Tokatli masonry bridge for situation 3, situation 4, and situation 5 are 3.96 cm, 5.89 cm, and 9.14 cm, respectively (Fig. 13). From these results, it is concluded that there is no significant seismic damage on the bridge during the earthquake for situations 1-5. In Fig. 14, the earthquake analysis results of the Tokatli bridge are presented for Case 6. According to Fig. 14, for situation 1 and situation 2, the largest seismic displacement values occurring on the Tokatli masonry stone bridge are 0.86 cm and 2.71 cm, respectively. In addition, the maximum displacement values observed on the bridge for situation 3 and situation 4 are 5.07 cm and 7.76 cm, respectively. Since the displacement values on the bridge for situations 1-4 are less than 10 cm, it is inferred that significant seismic damage did not occur on the bridge during the earthquake. However, for situation 6, the largest

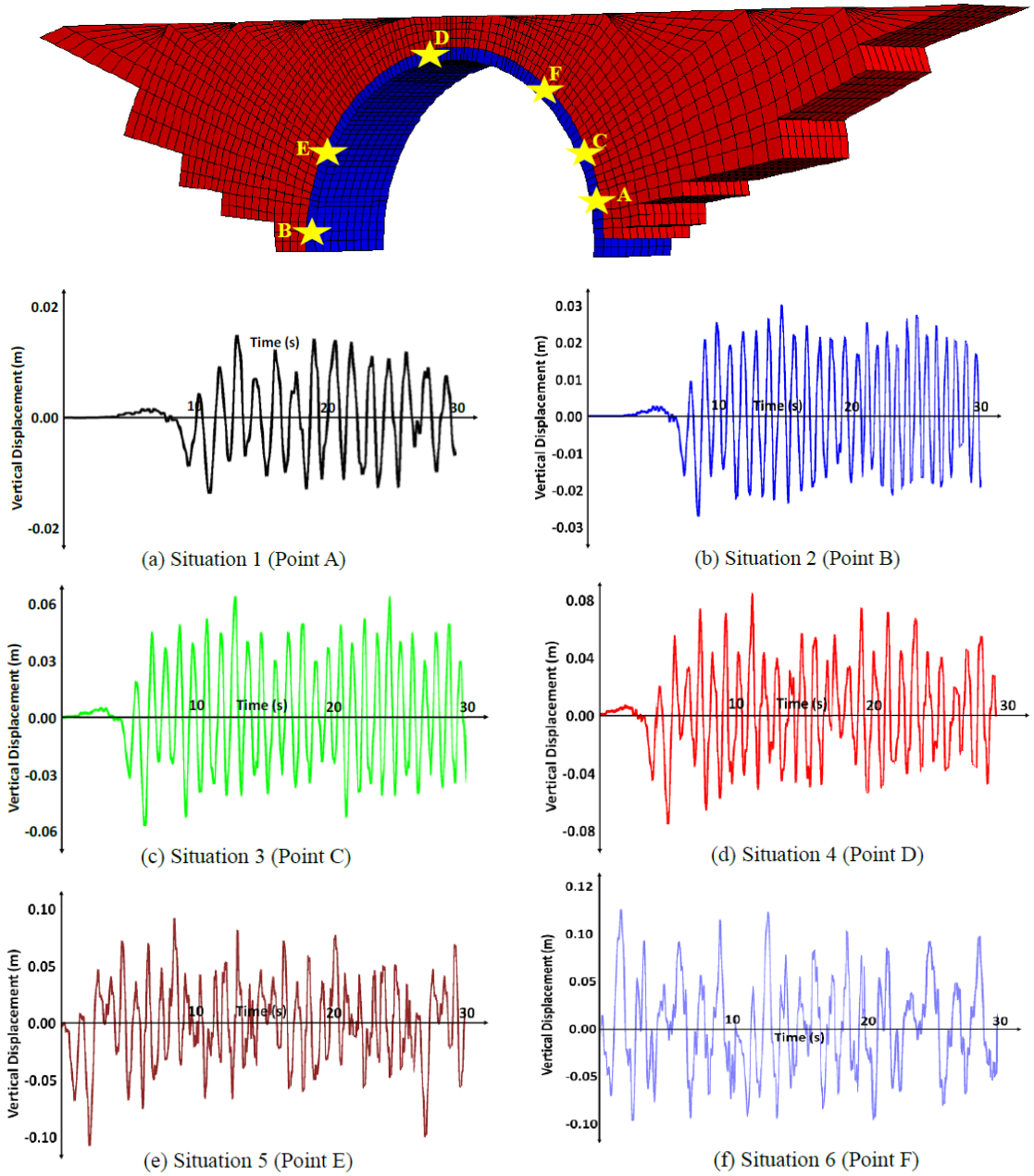

Fig. 12 Nonlinear seismic displacement results of the bridge for Case 4

seismic displacement value on the bridge is close to 10 cm, and earthquake reinforcement is recommended for situation 6. Besides, very critical cracks are gained in the middle of the arch material section of the bridge. From this result, it is suggested that the arch material part is very important during the earthquake and the arch material sections should be carefully strengthened for the seismic safety of the historical bridges. Fig. 15 shows the seismic analysis results of the Tokatli bridge for Case 7. According to Fig. 15, the vertical displacements that took place in the middle sections of the bridge are much larger than in other sections of the bridge. For situation 6, the maximum vertical displacement obtained on the bridge's body is approximately 9.91 cm. Besides, it is concluded that the vertical displacement values acquired during the earthquake for situation 5 and situation 6 are close to each other. Close vertical displacement values are obtained for situation 1 and situation 2. The largest displacement values on the bridge for situation 1 and situation 2 are 2.97 cm and 3.88 cm, respectively. Besides, the maximum seismic displacement values observed on the bridge body for situation 3, situation 4, and situation 5 are 5.83 cm, 7.94 cm, and 8.72 cm, respectively. For situation 6, the maximum seismic displacement value on the bridge is 9.91 cm.

The seismic analysis results for Case 8 are shown in Fig. 16 and it is seen that the most critical seismic cracks for the full reservoir situation occurred in the middle of the arch material section. Besides, during the earthquake, serious vertical displacements are observed on the underside of the arch material section. The maximum vertical displacement value obtained during the earthquake for situation 6 is approximately 10.94 cm. This seismic displacement value

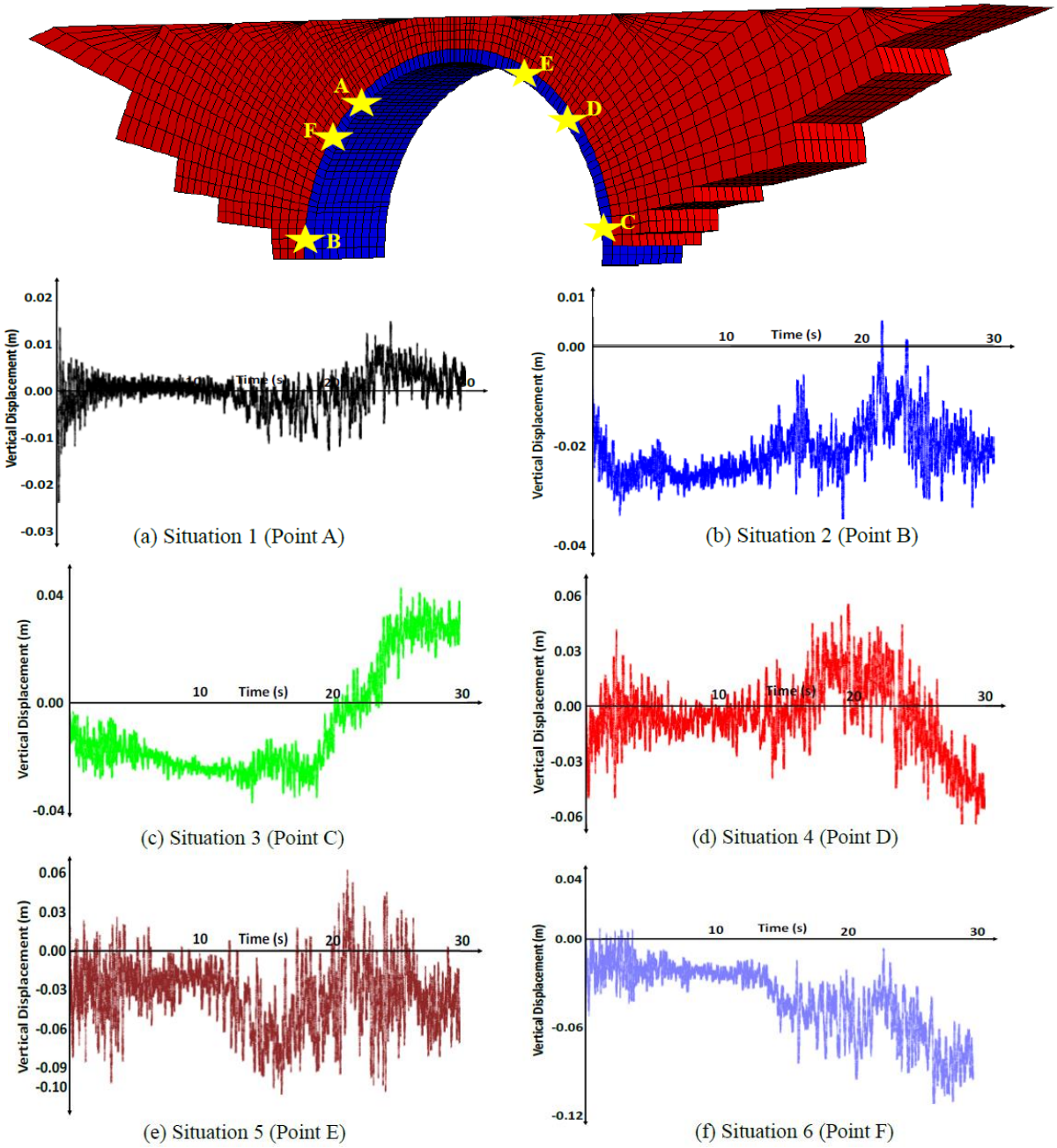

Fig. 13 Nonlinear seismic displacement results of the bridge for Case 5

can cause significant seismic damage to the bridge. For situation 5, seismic displacement values similar to situation 6 are obtained. During the earthquake, approximately 8.69 cm maximum displacement value is acquired on the bridge body for situation 5, and no seismic damage occurred on the bridge for situation 5. For situation 3 and situation 4, the maximum displacement values on the bridge body are 5.67 cm and 7.74 cm, respectively. Besides, the vertical displacement values acquired for situation 1 and situation 2 are very close to each other. The seismic displacement values of the bridge for situation 1 and situation 2 are 1.82 cm and 3.74 cm, respectively. As situation 1 and situation 6 are compared with each other, the effects of the reservoir water on the seismic behavior of the Tokatli bridge are seen (Fig. 16). In Fig. 17, three-dimensional earthquake analysis results are shown for Case 9. For Case 9, the maximum vertical displacement gained for the full reservoir condition on the bridge's body is approximately 10.59 cm. Furthermore, smaller vertical displacements are observed at the feet of the bridge when compared to the other sections of the bridge. Similar seismic displacement values are observed on the bridge for situation 5 and situation 6. The maximum displacement on the bridge for situation 5 is approximately 10.45 cm. This result shows that seismic damages may occur in the bridge body during the earthquake for situation 5 and situation 6. Moreover, the seismic displacement values observed on the bridge for situation 3 and situation 4 are 4.97 cm and 6.58 cm, respectively. It is observed that the maximum displacement values obtained on the bridge for situation 1 and situation 2

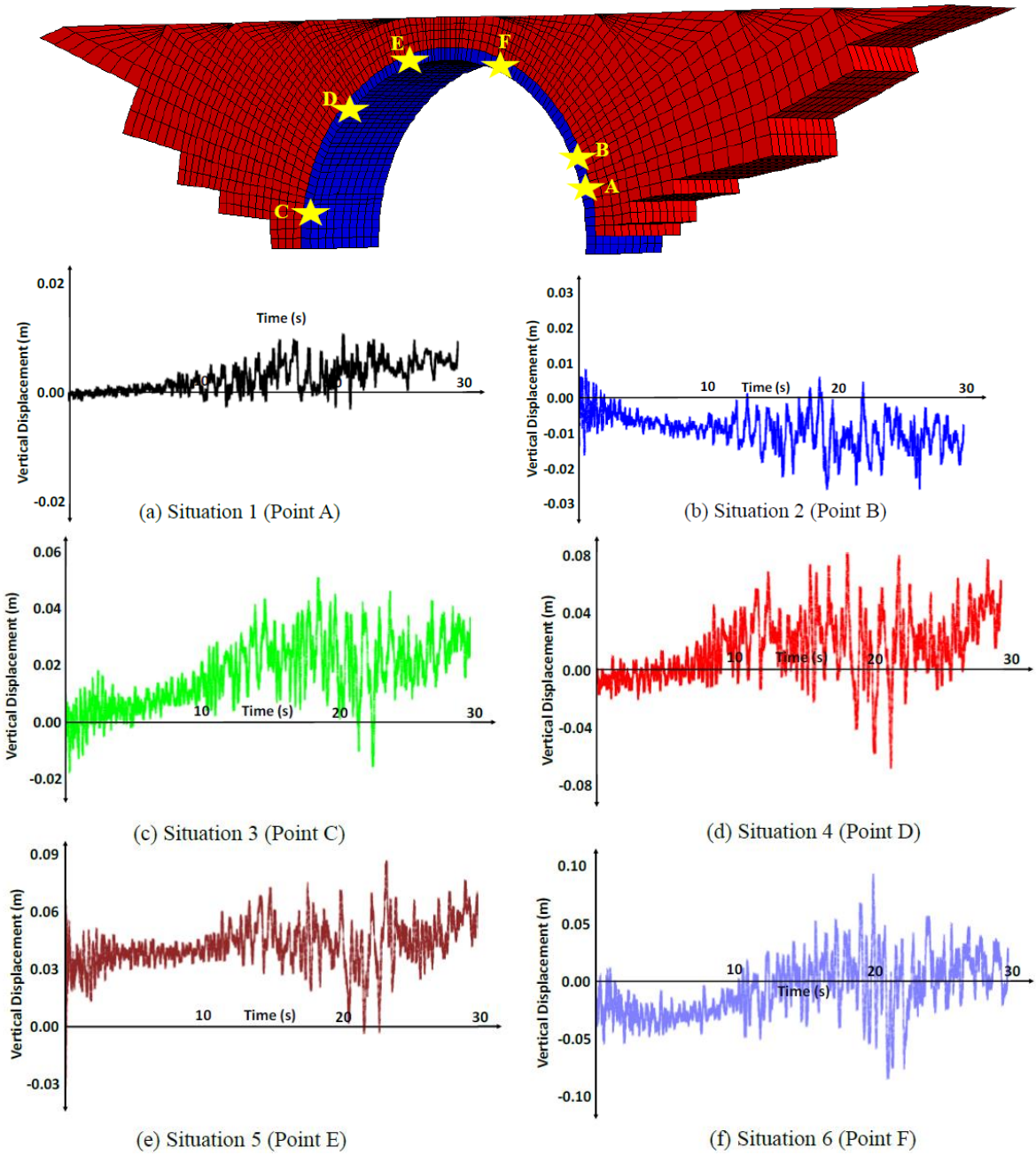

Fig. 14 Nonlinear seismic displacement results of the bridge for Case 6

are smaller than in other situations. The largest seismic displacement values on the Tokatli bridge for situation and situation 2 are 1.65 cm and 3.48 cm, respectively (Fig. 17). The seismic analysis results gained for Case 10 are presented in Fig. 18. As Case 10 is examined in detail, it is concluded that the vertical displacements that occurred for the full reservoir condition of the bridge are much larger than the empty reservoir condition of the bridge. For Case 10, it is observed that the most critical cracks in the bridge occurred in the arch material section of the bridge. Also, insignificant cracks are observed at the bridge feet. The largest seismic displacement values observed on the bridge for situation 1 and situation 2 are 1.36 cm and 3.87 cm, respectively. In addition, the maximum seismic displacement values in the bridge body for situation 3 and situation 4 are 5.76 cm and 6.08 cm, respectively. It is clear from these results that no seismic damages occurred in the bridge body during the earthquake for situations 1-4. For situation 5 and situation 6, the largest seismic displacement values on the bridge are 9.83 cm and 10.77 cm, respectively. The seismic displacement values obtained for situation 5 and situation 6 caused significant seismic damage to the bridge body. For this reason, seismic reinforcement of the bridge body is recommended for situation 5 and situation 6 (Fig. 18). Fig. 19 shows the seismic principal stress results of the Tokatli masonry stone arch bridge. The results are obtained by considering 10 different earthquakes and 6 different water levels. When the results are evaluated in general, it is clear that the change in water level significantly changed the principal stress

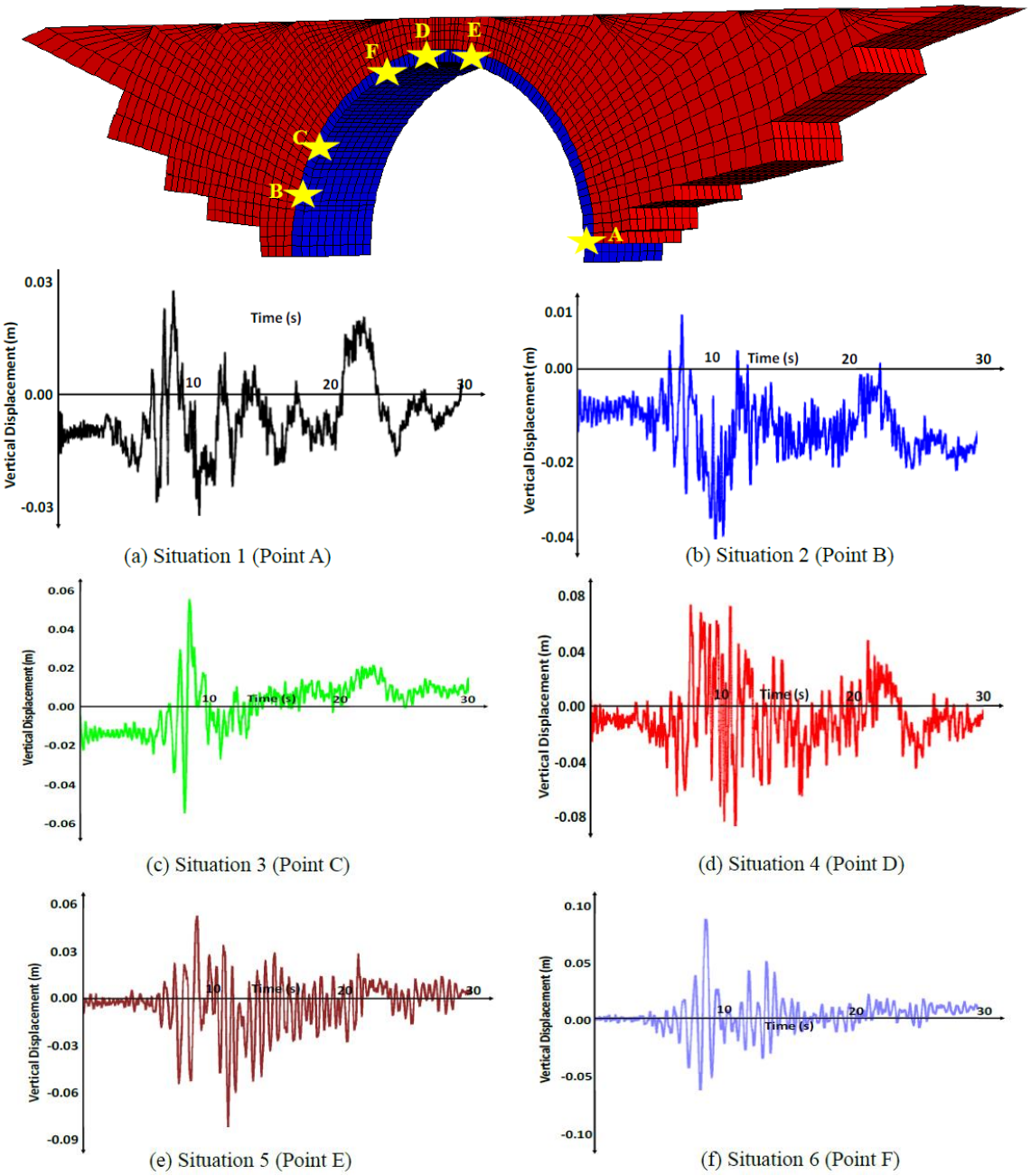

Fig. 15 Nonlinear seismic displacement results of the bridge for Case 7

behavior of the bridge. For situation 1, situation 2, and situation 3, the seismic principal stress values on the bridge are close to each other. However, the principal stress values on the bridge increased significantly after the water came into contact with the bridge body. When situation 4, situation 5, and situation 6 are compared with each other, it is openly seen that the highest principal stress values on the bridge during the earthquake took place for situation 6. Moreover, Yazdani and Habibi (2021) stated that if the principal stress values of masonry bridges are greater than 6.9 MPa, significant damage may occur in masonry bridges. When 10 different earthquake analyzes are examined in line with this suggestion, it is concluded that no significant seismic damage occurred in the bridge body during the strong ground motions.

5. Conclusions

Historical bridges have met the water needs of many civilizations and humanity, and they have provided safe transportation. These structures are of great importance both in terms of tourism and the history of countries today. For this reason, both long-term creep behavior and three-dimensional seismic analyzes of masonry stone arch bridges are investigated considering the finite-difference method in this study. The Tokatli historical stone arch bridge, which was built in Karabük-Turkey in 1179, is chosen for the numerical analyses. Firstly, the long-term creep behavior of the bridge is investigated from 1179 to 2022. While examining the creep behavior of the bridge, the Burgers-Creep criteria and fix boundary condition are utilized. Then,

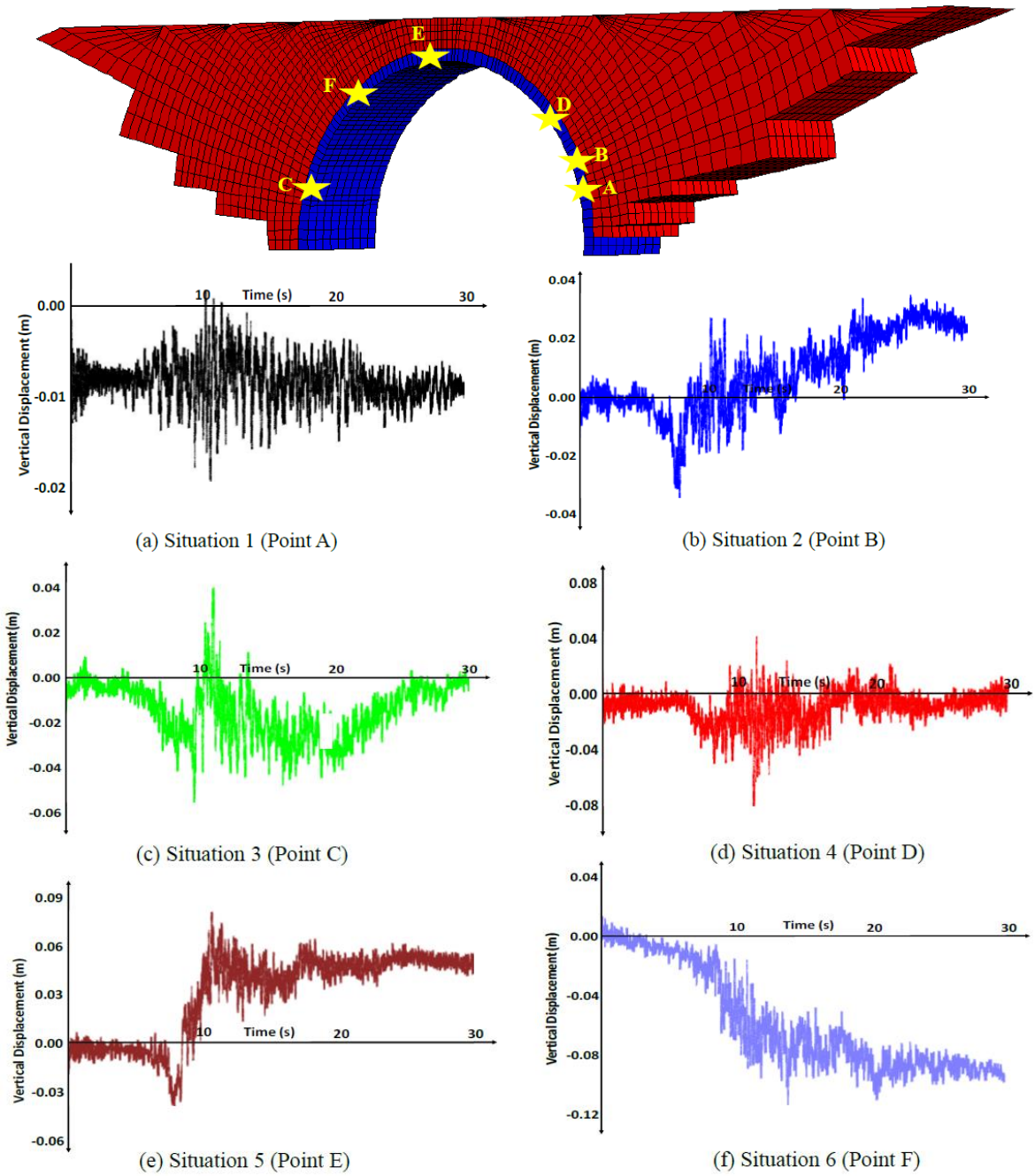

Fig. 16 Nonlinear seismic displacement results of the bridge for Case 8

the seismic behavior of the bridge is interpreted using 10 various ground motions. While performing seismic analyses, the free-field and quiet boundary conditions are taken into account. According to the creep and seismic analysis results examined under different water heights, the following important results are obtained.

- Considering 6 different water heights, it has been understood that each water height has separate creep and seismic effects on the structural behavior of the bridge. According to the creep analysis results, it is understood that the largest vertical displacements that occurred on the bridge during 843 years are acquired for the full reservoir condition of the bridge. Furthermore, the smallest vertical displacements in the bridge are observed for the empty reservoir of the bridge. For situation 1 (empty reservoir) and situation 2, the maximum creep displacement values on the bridge over 843 years are 0.44 cm and 0.73 cm, respectively. Moreover, the maximum creep displacement values observed on the bridge for situation 3, situation 4, situation 5, and situation 6 (full reservoir) are 1.67 cm, 4.05 cm, 5.2 cm, and 6.05 cm, respectively. According to the 843-year creep analysis results, no significant creep damage has occurred in the Tokatli bridge for 6 various water levels.
- According to 10 different seismic analysis results, it has been observed that the largest vertical displacements are obtained for the full reservoir

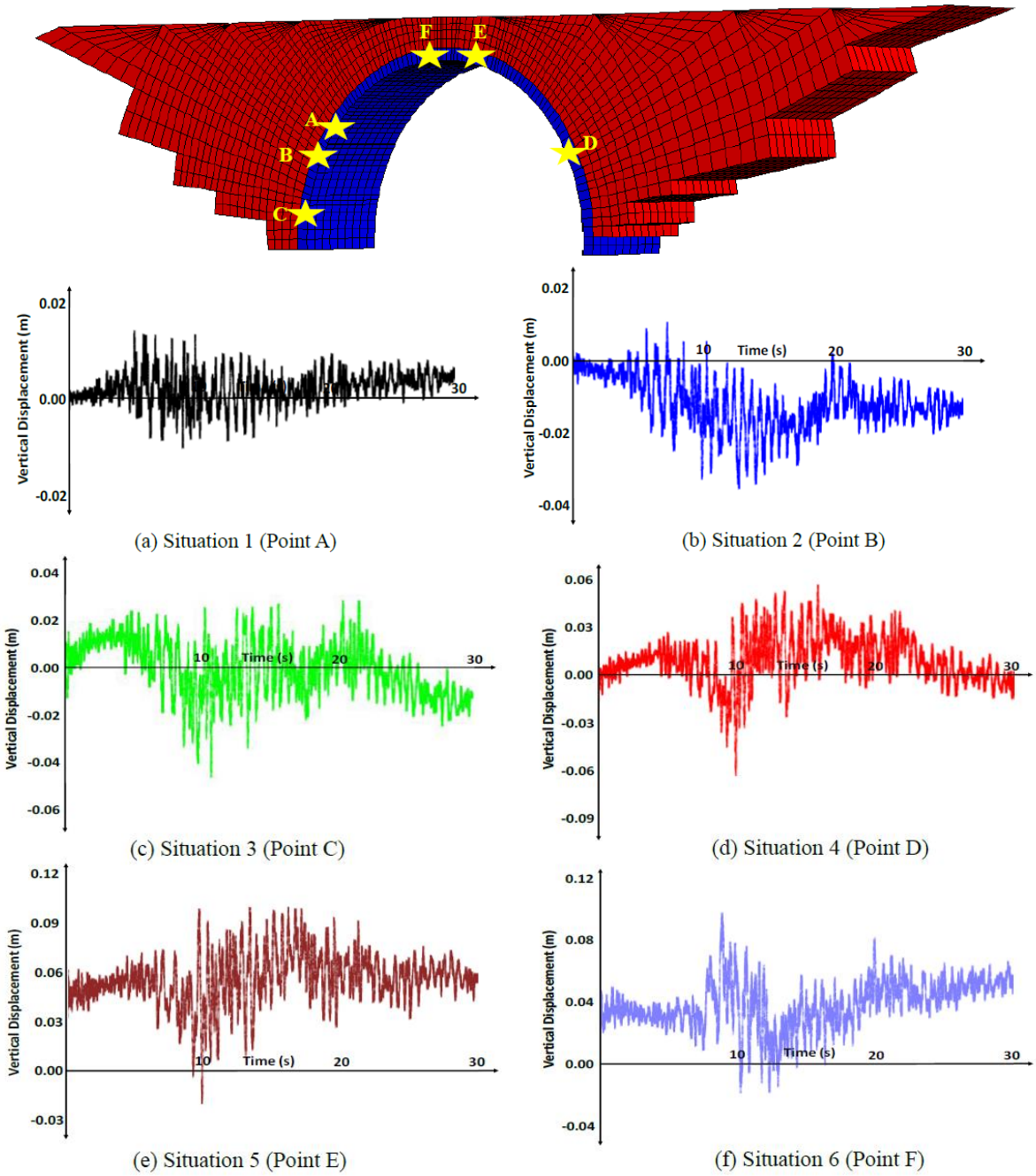

Fig. 17 Nonlinear seismic displacement results of the bridge for Case 9

situation. Besides, it is concluded that the smallest vertical displacements took place for the empty reservoir situation. This result shows that when the water height increases, the seismic vertical displacements that occurred in the bridge's body increase. Close seismic vertical displacements are observed for situations 1, 2, and 3. It is clear from this result that if the water does not come into contact with the bridge's body, there is no significant effect on the seismic vertical displacement behavior of the bridge.

- According to the seismic analysis results of the Tokatli bridge, the seismic displacement values of the bridge's body for 10 different earthquakes are less than 10 cm. For this reason, it is concluded that the bridge was not exposed to significant seismic damage during the earthquake. However, in some earthquake analyses, it is observed that the seismic displacement values of the bridge body for situation 6 (full reservoir) are greater than 10 cm. For situation 6, seismic reinforcement of the bridge's body is recommended.
- When the literature is examined, it is seen that the maximum principal stress value that masonry bridges can withstand earthquake loads is 6.9 MPa. For 10 various earthquake analyses, the greatest principal stress values occurring on the Tokatli bridge during the earthquake are less than 6.9 MPa. For this reason, principal stress damages did not occur in the Tokatli bridge during 10 different earthquakes.

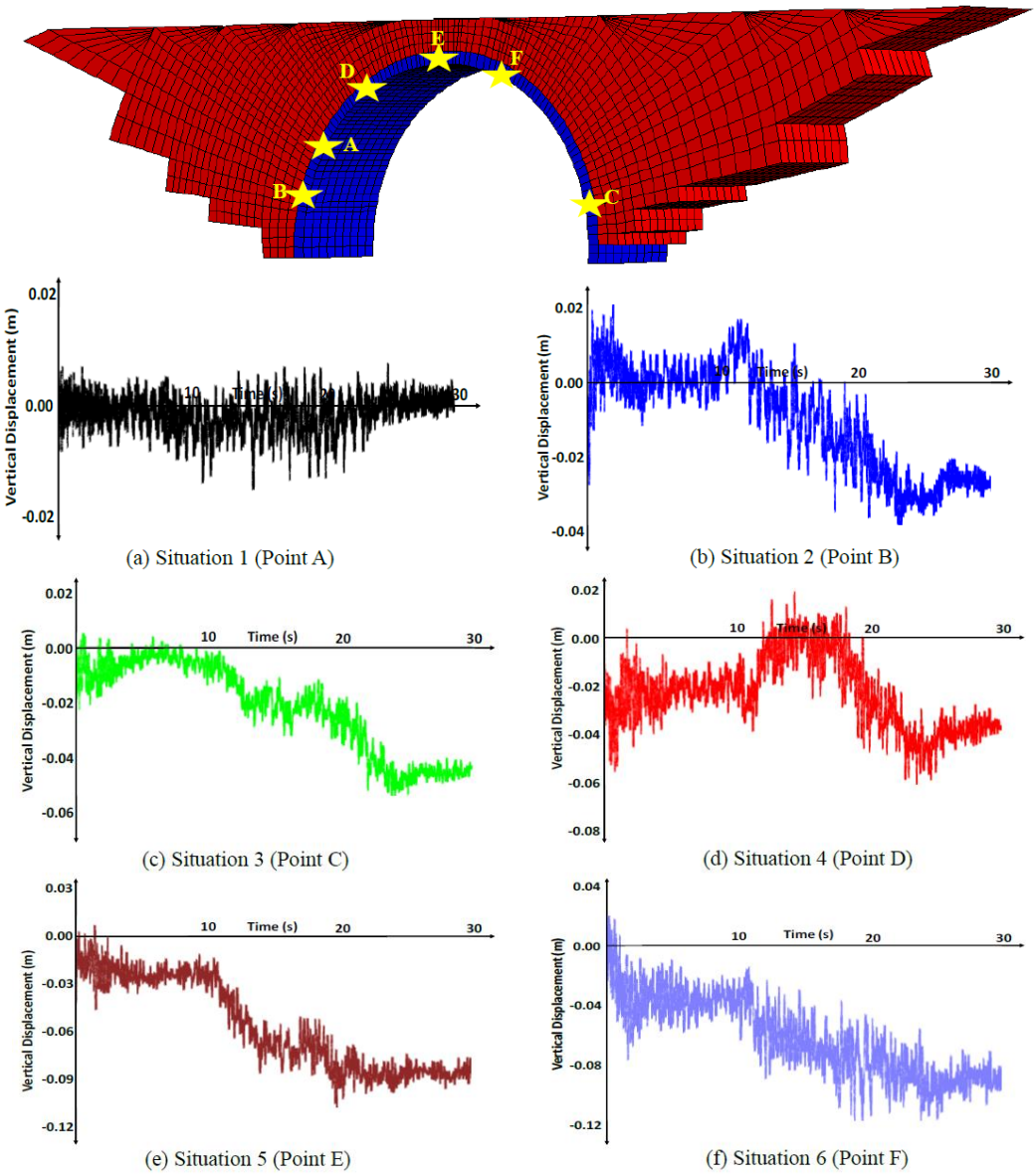

Fig. 18 Nonlinear seismic displacement results of the bridge for Case 10

- The water level significantly changed the seismic principal stress values on the bridge. The largest seismic principal stress values on the bridge are obtained for situation 6. Besides, the stress values on the bridge for situations 5 and 6 are close to each other. The smallest principal stress values observed on the bridge body are acquired for situation 1.
- It is concluded that the water height significantly changed the creep and seismic behavior of historical bridges. For this reason, it is suggested that the height of the water should be taken into account while analyzing and modeling historical bridges built in seismic zones and flood zones.

References

Aydin, A.C. and Özkaya, S.G. (2018), "The finite element analysis of collapse loads of single-spanned historic masonry arch bridges (Ordu, Sarpdere Bridge)", *Eng. Fail. Anal.*, **84**, 131-138. https://doi.org/10.1016/j.engfailanal.2017.11.002.

Cakir, F. and Seker, B.S. (2015), "Structural performance of renovated masonry low bridge in Amasya, Turkey", *Earthq. Struct.*, **8**(6), 1387-1406. https://doi.org/10.12989/eas.2015.8.6.1387.

Cavuslu, M. (2022), "3D seismic assessment of historical stone arch bridges considering effects of normal-shear directions of stiffness parameters between discrete stone elements", *Struct. Eng. Mech.*, **83**(2), 207-227. https://doi.org/10.12989/sem.2022.83.2.207.

Conde, B., Díaz-Vilariño, L., Lagüela, S. and Arias, P. (2016), "Structural analysis of Monforte de Lemos masonry arch bridge considering the influence of the geometry of the arches and fill material on the collapse load estimation", *Constr. Build. Mater.*, **120**, 630-642. https://doi.org/10.1016/j.conbuildmat.2016.05.107.

Costa, C., Arêde, A., Morais, M. and Aníbal, A. (2015), "Detailed FE and DE modelling of stone masonry arch bridges for the assessment of load-carrying capacity", *Procedia Eng.*, **114**, 854-861. https://doi.org/10.1016/j.proeng.2015.08.039.

Dogan, M. (2013), "Failure of structural (RC, masonry, bridge) to

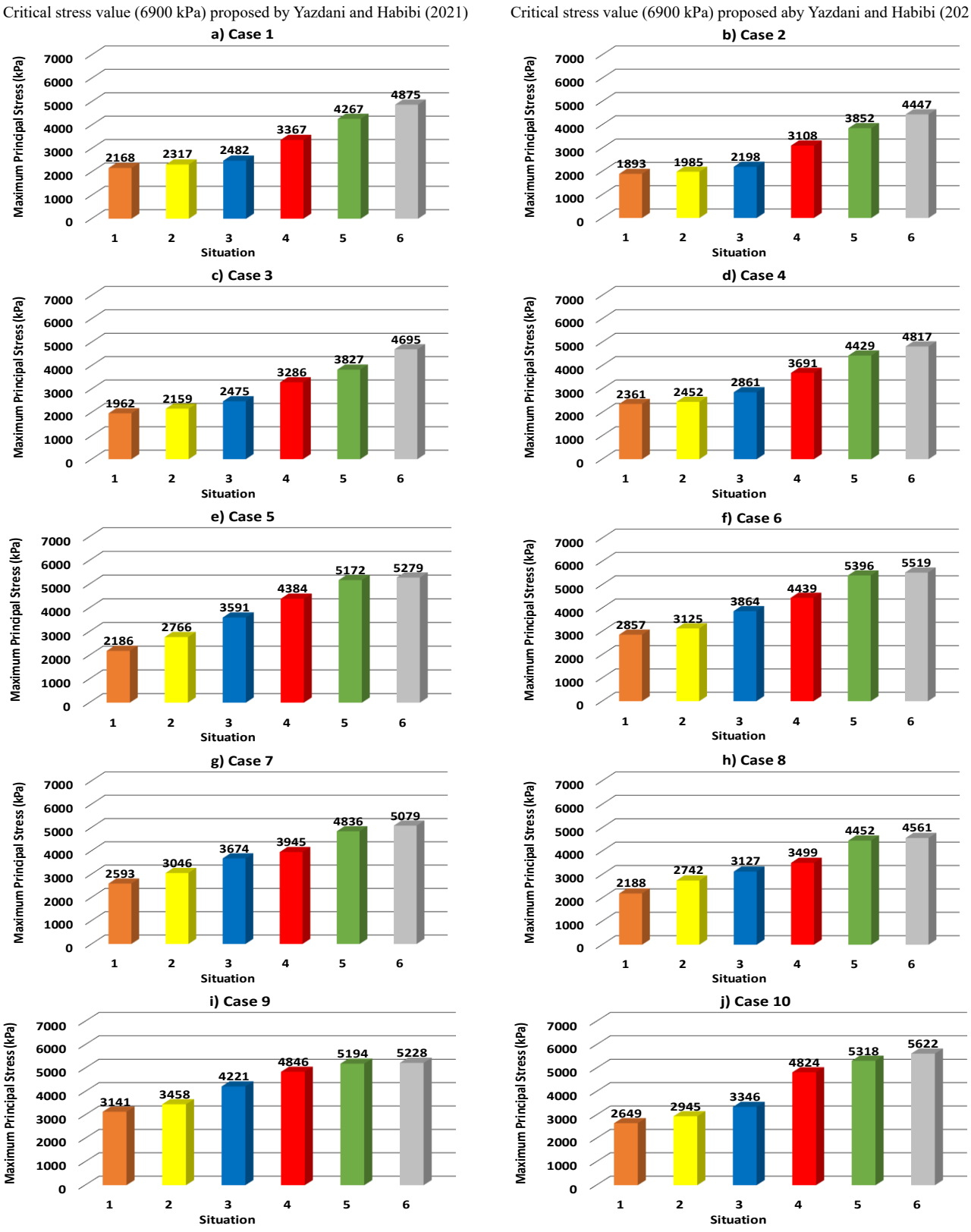

Fig. 19 Seismic principal stress results on the arch section of Tokatli bridge for different earthquakes

Van earthquake", *Eng. Fail. Anal.*, **35**, 489-498. https://doi.org/10.1016/j.engfailanal.2013.05.010.

Domede, N., Sellier, A. and Stablon, T. (2013), "Structural analysis of a multi-span railway masonry bridge combining in situ observations, laboratory tests and damage modelling", *Eng. Struct.*, **56**, 837-849. https://doi.org/10.1016/j.engstruct.2013.05.052.

Fanack (2022), Retrieved January 10, 2022, from https://fanack.com/turkey/geography-of-turkey/.

Forgács, T., Sarhosis, V. and Ádány, S. (2021), "Shakedown and dynamic behaviour of masonry arch railway bridges", *Eng.*

Struct., **228**, 111474. https://doi.org/10.1016/j.engstruct.2020.111474.
Gonen, H., Dogan, M., Karacasu, M., Ozbasaran, H. and Gokdemir, H. (2013), "Structural failures in refrofit historical murat masonry arch bridge", *Eng. Fail. Anal.*, **35**, 334-342. https://doi.org/10.1016/j.engfailanal.2013.02.024.
Gönen, S. and Soyöz, S. (2021), "Seismic analysis of a masonry arch bridge using multiple methodologies", *Eng. Struct.*, **226**, 111354. https://doi.org/10.1016/j.engstruct.2020.111354.
Google Earth (2022), Retrieved January 10, 2022, from https://earth.google.com/web/.
Hacıefendioğlu, K. and Koç, V. (2016), "Dynamic assessment of partially damaged historic masonry bridges under blast-induced ground motion using multi-point shock spectrum method", *Appl. Math. Model.*, **40**(23-24), 10088-10104. https://doi.org/10.1016/j.apm.2016.06.049.
Itasca (2002), Inc. FLAC Version 5 User Manual, Minneapolis, USA.
Jiang, K. and Esaki, T. (2002), "Quantitative evaluation of stability changes in historical stone bridges in Kagoshima, Japan, by weathering", *Eng. Geol.*, **63**(1-2), 83-91. https://doi.org/10.1016/S0013-7952(01)00071-0.
Karalar, M. and Cavuslu, M. (2022), "Determination of 3D near fault seismic behaviour of Oroville earth fill dam using burger material model and free field-quiet boundary conditions", *Math. Comput. Model. Dyn. Syst.*, **28**(1), 55-77. https://doi.org/10.1080/13873954.2022.2033274.
Karaton, M., Aksoy, H.S., Sayın, E. and Calayır, Y. (2017), "Nonlinear seismic performance of a 12th century historical masonry bridge under different earthquake levels", *Eng. Fail. Anal.*, **79**, 408-421. https://doi.org/10.1016/j.engfailanal.2017.05.017.
Milani, G. and Lourenço, P.B. (2012), "3D non-linear behavior of masonry arch bridges", *Comput. Struct.*, **110-111**, 133-150. https://doi.org/10.1016/j.compstruc.2012.07.008.
Onat, O. (2019), "Fundamental vibration frequency prediction of historical masonry bridges", *Struct. Eng. Mech.*, **69**(2), 155-162. https://doi.org/10.12989/sem.2019.69.2.155.
Panian, R. and Yazdani, M. (2020), "Estimation of the service load capacity of plain concrete arch bridges using a novel approach: Stress intensity factor", *Struct.*, **27**, 1521-1534. https://doi.org/10.1016/j.istruc.2020.07.055.
Pelà, L., Aprile, A. and Benedetti, A. (2009), "Seismic assessment of masonry arch bridges", *Eng. Struct.*, **31**(8), 1777-1788. https://doi.org/10.1016/j.engstruct.2009.02.012.
Pelà, L., Aprile, A. and Benedetti, A. (2013), "Comparison of seismic assessment procedures for masonry arch bridges", *Constr. Build. Mater.*, **38**, 381-394. https://doi.org/10.1016/j.conbuildmat.2012.08.046.
Sarhosis, V., Forgács, T. and Lemos, J.V. (2018), "A discrete approach for modelling backfill material in masonry arch bridges", *Comput. Struct.*, **224,** 106108. https://doi.org/10.1016/j.compstruc.2019.106108.
Saygılı, Ö. and Lemos, J.V. (2021), "Seismic vulnerability assessment of masonry arch bridges", *Struct.*, **33**, 3311-3323. https://doi.org/10.1016/j.istruc.2021.06.057.
Sayin, E. (2015), "Nonlinear seismic response of a masonry arch bridge", *Earthq. Struct.*, **10**(2), 483-494. https://doi.org/10.12989/eas.2016.10.2.483.
Spyrakos, C.C., Kemp, E.L. and Venkatareddy, R. (1999), "Seismic study of an historic covered bridge", *Eng. Struct.*, **21**(9), 877-882. https://doi.org/10.1016/S0141-0296(98)00041-8.
Tubaldi, E., Macorini, L. and Izzuddin, B.A. (2018), "Three-dimensional mesoscale modelling of multi-span masonry arch bridges subjected to scour", *Eng. Struct.*, **165**, 486-500. https://doi.org/10.1016/j.engstruct.2018.03.031.
Türker, T. (2014), "Structural evaluation of Aspendos (Belkis) Masonry Bridge", *Struct. Eng. Mech.*, **50**(4), 419-439. https://doi.org/10.12989/sem.2014.50.4.419.
Ural, A., Oruç, Ş., Doğangün, A. and Tuluk, Ö.İ. (2008), "Turkish historical arch bridges and their deteriorations and failures", *Eng. Fail. Anal.*, **15**(1-2), 43-53. https://doi.org/10.1016/j.engfailanal.2007.01.006.
Wang, L., Wang, S., Li, G. and Wang, L. (2020), "Construction of 3D creep model of landslide slip-surface soil and secondary development based on FLAC3D", *Adv. Civil Eng.*, **2020**, Article ID 2694651. https://doi.org/10.1155/2020/2694651.
Yazdani, M. (2021), "Three-dimensional nonlinear finite element analysis for load-carrying capacity prediction of a railway arch bridge", *Int. J. Civil Eng.*, **19**, 823-836. https://doi.org/10.1007/s40999-021-00608-w.
Yazdani, M. and Habibi, H. (2021), "Residual capacity evaluation of masonry arch bridges by extended finite element method", *Struct. Eng. Int.*, 1-12. https://doi.org/10.1080/10168664.2021.1944454.
Yazdani, M. and Jahangiri, V. (2020), "Intensity measure-based probabilistic seismic evaluation and vulnerability assessment of ageing bridges", *Earthq. Struct.*, **19**(5), 379-393. https://doi.org/10.12989/eas.2020.19.5.379.
Yazdani, M., Jahangiri, V. and Marefat, M.S. (2019), "Seismic performance assessment of plain concrete arch bridges under near-field earthquakes using incremental dynamic analysis", *Eng. Fail. Anal.*, **106**, 104170. https://doi.org/10.1016/j.engfailanal.2019.104170.
Yeşil, M. (2019), "Investigation of behavior change of conjic and tokatli historical masonry stone bridges with different openings and belt height under near and far fault using the finite element method ansys and Sap2000", *Zonguldak Bülent Ecevit University Graduate School of Natural and Applied Sciences*, June.
Zampieri, P., Tetougueni, C.D. and Pellegrino, C. (2021), "Nonlinear seismic analysis of masonry bridges under multiple geometric and material considerations: Application to an existing seven-span arch bridge", *Struct.*, **34**, 78-94. https://doi.org/10.1016/j.istruc.2021.07.009.

CC